

Non-collinear magnetic structures: a possible cause for current induced switching

P. Weinberger¹⁾, A. Vernes¹⁾, B. L. Györffy^{1,2)}, and L. Szunyogh^{1,3)}

¹⁾ *Center for Computational Materials Science,
Gumpendorferstr. 1a, A-1060 Vienna, Austria*

²⁾ *H. H. Wills Physics Laboratory, Bristol University,
Royal Fort, Tyndall Avenue, Bristol BS8 1TL, U. K.*

³⁾ *Department of Theoretical Physics,
Center for Applied Mathematics and Computational Physics,
Budapest University of Technology and Economics,
Budafoki út. 8, H-1521 Budapest, Hungary*

(Dated: April 21, 2004)

Abstract

Current induced switching in Co/Cu/Co trilayers is described in terms of ab-initio determined magnetic twisting energies and corresponding sheet resistances. In viewing the twisting energy as an energy flux the characteristic time thereof is evaluated by means of the Landau-Lifshitz-Gilbert equation using ab-initio parameters. The obtained switching times are in very good agreement with available experimental data. In terms of the calculated currents, scalar quantities since a classical Ohm's law is applied, critical currents needed to switch magnetic configurations from parallel to antiparallel and vice versa can unambiguously be defined. It is found that the magnetoresistance viewed as a function of the current is essentially determined by the twisting energy as a function of the relative angle between the orientations of the magnetization in the magnetic slabs, which in turn can also explain in particular cases the fact that after having switched off the current the system remains in the switched magnetic configuration. For all ab-initio type calculations the fully relativistic Screened Korringa-Kohn-Rostoker method and the corresponding Kubo-Greenwood equation in the context of density functional theory are applied.

PACS numbers: 75.30.Gw, 75.70.Ak, 75.70.Cn

I. INTRODUCTION

Reversal of the orientation of the magnetization without applying an external field seems to be of considerable interest for magnetic switching of micro-devices and caused extensive experimental and theoretical studies of the effect of currents on magnetic nanostructures. The experimental facts^{1,2,3,4,5,6,7,8,9,10,11,12,13} are still quite confusing, or, to put in the words of a recent short review article¹⁴, "many observed phenomena can be described qualitatively ... by a simple semi-classical spin-torque model. However, evidence of complications from several experiments suggests that a full understanding of all observations is not yet achieved". The by now generally accepted experimental facts are the following ones: (1) if the current of a given sign favors the parallel (P) magnetic configuration, the current of the opposite sign favors the antiparallel (AP) configuration, (2) the current needed to switch the magnetic configuration in nanostructured magnetic multilayer systems is of the order of 2 - 5 mA in samples with a volume in the range of 40 - 800 nm³. These two facts led *inter alia* to a schematic effective two-level energy diagram for switching in which the critical current corresponds to the energy needed to overcome the potential barrier between the parallel and the antiparallel magnetic configuration. Since experimentally also telegraph noise is observed, which in turn seems to correspond to an oscillation between these two states, this schematic picture proved to be quite useful. If by means of a sufficiently high current the system is driven from one configuration to the other one, it also can happen that after turning off the current the system remains in the switched configuration, i.e., the system does not return to the ground state. In the two-level energy diagram this would correspond to the case that the two schematic minima are separated by a high enough potential barrier and are of about the same energy.

Most theoretical investigations^{15,16,17,18,19,20,21,22,23,24,25} were concerned about finding expressions for the interaction between the applied current and the orientation of the magnetic moments. Almost all theoretical considerations and models used the concept of spin currents and had to use phenomenological parameters to relate the respective approach to the experimental evidence. Quite clearly in most cases the main idea was to describe the cause for current induced switching and deal afterwards with the subsequent effect, namely a change in the magnetoresistance. Therefore the effect – creating excited states – was interpreted in various ways by invoking spin waves, all kinds of spin-polarization effects, etc. It is be-

yond the scope of the present paper to summarize the various theoretical approaches used up-to-now.

In here a completely different approach is pursued: the main idea is to calculate fully relativistically the twisting (exchange interaction) energy of a system as it goes from a parallel to an antiparallel configuration, or opposite. This is a continuous function of the relative angle between the orientations of the magnetization in the magnetic parts of a spin valve system. In keeping one orientation fixed and rotating the other one by an angle Θ around an axis perpendicular to the fixed orientation one thus can switch continuously from say the parallel magnetic configuration to the antiparallel configuration. For each given rotation angle Θ simultaneously the corresponding sheet resistance (resistance divided by the unit area) is calculated fully relativistically, which then is also a continuous function of the rotation angle. It should be noted that by using a fully relativistic approach the spin no longer is an observable, i.e., at a given angle Θ there is just one sheet resistance. In adopting this approach (1) the excitation energy is related to the rotation angle, and (2) for the same angle a physical observable, namely the sheet resistance is evaluated. Therefore at a given Θ the effect of the physical phenomenon is described, which then can be related to the cause, namely the turning on of a current. It will be shown later on that the twisting (exchange interaction) energy is the ab-initio analogon of the above mentioned two-level energy diagram for switching. Furthermore, by means of relating the twisting energy and the corresponding sheet resistance to the current not only a critical current can be defined unambiguously, but also the complexity of the switching process becomes evident. Quite clearly in this picture no dynamic effects can be calculated, although very good reasons for the occurrence of the telegraph noise can be given. The quantum mechanical tools applied are the fully relativistic screened Korringa-Kohn-Rostoker method²⁶ and the fully relativistic Kubo-Greenwood equation²⁷ in the context of the local density functional approximation. All further reasoning is based on the Landau-Lifshitz-Gilbert equation, in terms of which switching times can be evaluated using ab-initio parameters. The introduced approach is applied to Co/Cu/Co type spin valves and in fact will show quite a few of the experimentally observed features mentioned earlier.

II. TWISTING ENERGIES AND SHEET RESISTANCES

Consider a typical trilayer system of the type FM/NM_n/FM consisting of two semi-infinite magnetic leads (FM) and a so-called non-magnetic spacer (NM) such as for example Co(100)/Cu_n/Co(100) or equivalently Co(100)/Cu_n/Co_m/Vac, where n denotes the number of spacer layers and m is a sufficiently large number of layers of the magnetic metal. Suppose now that \vec{n}_0 denotes a particular unit vector (reference orientation, either parallel or perpendicular to the surface normal) characterizing the orientation of the magnetization in a particular atomic layer containing one atom per unit cell. If

$$\vec{n}_B = \vec{n}_{B'} = \vec{n}_i = \vec{n}_0 \quad , \quad i = 1, \dots, n \quad , \quad (1)$$

such a configuration is usually referred to as a parallel configuration, whereas for

$$\vec{n}_B = \vec{n}_i = \vec{n}_0 \quad , \quad i = 1, \dots, (n/2) \quad ; \quad \vec{n}_{B'} = \vec{n}_i = -\vec{n}_0 \quad , \quad i = (n/2) + 1, \dots, n \quad , \quad (2)$$

frequently the term “symmetric” antiparallel configuration is used. If $\vec{n}_B, \vec{n}_{B'}$ (the orientations of the magnetization in the semi-infinite leads) and the \vec{n}_i are each rotated by individual angles around an axis perpendicular to \vec{n}_0 this situation refers to a general non-collinear magnetic configuration in two-dimensional translational invariant systems. As for reasonably large n the interior of the NM part is completely non-magnetic in the following specific non-collinear configurations of the type

$$\vec{n}_B = \vec{n}_i = \vec{n}_0 \quad , \quad i = 1, \dots, (n/2) \quad ; \quad \vec{n}_{B'} = \vec{n}_i = \vec{n}'_0 \quad , \quad i = (n/2) + 1, \dots, n \quad , \quad (3)$$

will be considered, where \vec{n}'_0 is a unit vector rotated by an angle Θ with respect to \vec{n}_0 . It is obvious that for these magnetic configurations it is sufficient to specify the rotation angle Θ . Expressed in simple terms this means that in the right half of the trilayer system the orientation of the magnetization is rotated uniformly by an angle Θ with respect to the orientation of the magnetization in the left half.

Since a current perpendicular to the planes of atoms has to be described in the present paper the reference orientation \vec{n}_0 is chosen to be parallel to the surface normal (z axis); the rotations are performed around the y axis.

A. Twisting energies

The energy difference between the two possible collinear states, namely the parallel and the “symmetric” antiparallel magnetic configuration, is usually termed interlayer exchange coupling energy. In using the magnetic force theorem²⁸ the total energies of these states are replaced by the corresponding grand potentials (at zero temperature), i.e., by the so-called band energy difference $\Delta E_b^0(\pi)$,

$$\Delta E_b^0(\pi) = E_b(\pi) - E_b(0) = E_b(AP) - E_b(P) , \quad (4)$$

$$E_b(\Theta) = \int_{E_0}^{E_F} n(\Theta; E)(E - E_F)dE , \quad (5)$$

where $n(\Theta; E)$ is the density of states for a particular configuration, E_0 the valence band bottom and E_F the Fermi energy. According to Eq. (4) the below convention applies

$$\Delta E_b^0(\pi) = \begin{cases} > 0 & P : \text{ground state} \\ < 0 & AP : \text{ground state} \end{cases} . \quad (6)$$

In a similar manner the “twisting energy” is defined by the following difference,

$$\Delta E_b(\Theta) = E_b(\Theta) - E_b(0) , \quad 0 \leq \Theta \leq \pi , \quad (7)$$

and – as is well-known – can be expanded in a power series in $\cos \Theta$

$$\Delta E_b(\Theta) = a(1 - \cos(\Theta)) + b \cos^2(\Theta) + c \cos^3(\Theta) + \dots , \quad (8)$$

such that in all orders

$$a = \Delta E_b(\pi/2) . \quad (9)$$

In first order $\Delta E_b(\Theta)$ is then approximated by

$$\Delta E_b(\Theta) \sim \Delta E_b^{(1)}(\Theta) = a(1 - \cos(\Theta)) , \quad (10)$$

in second order by

$$\Delta E_b(\Theta) \sim \Delta E_b^{(2)}(\Theta) = a(1 - \cos(\Theta)) + b \cos^2(\Theta) , \quad b = \Delta E_b(\pi) - 2\Delta E_b(\pi/2) , \quad (11)$$

in third order by

$$\Delta E_b(\Theta) \sim \Delta E_b^{(3)}(\Theta) = a(1 - \cos(\Theta)) + b \cos^2(\Theta) + c \cos^3(\Theta) , \quad (12)$$

$$b = -\Delta E_b(\pi) - 2\Delta E_b(\pi/2) + 8\Delta E_b(2\pi/3) , \quad c = 8\Delta E_b(2\pi/3) - 2\Delta E_b(\pi) , \quad (13)$$

etc., where $\Delta E_b(\pi)$, $\Delta E_b(\pi/2)$, \dots , refer to the actually calculated values.

It should be noted that most frequently $\Delta E_b(\Theta) \sim \Delta E_b^{(1)}(\Theta)$ is assumed, an approximation, which – as will be shown later on – not necessarily is granted. Clearly enough in using only $\Delta E_b^{(1)}(\Theta)$ the coefficient a is simply half of the interlayer exchange coupling energy, $a = \Delta E_b^{(1)}(\pi)/2$. In principle by calculating $\Delta E_b(\Theta)$ for a few selected values of Θ , in terms of Eq. (8) a reasonably good approximation to $\Delta E_b(\Theta)$ for Θ varying continuously between 0 and π can be obtained.

B. Sheet resistance and magnetoresistance

As is well-known in CPP (current perpendicular to the planes of atoms geometry) the magnetoresistance can be defined via the sheet resistances for the respective collinear magnetic configurations P and AP ,

$$MR(\pi) = \frac{\Delta r(\pi)}{r(\pi)} = \frac{r(\pi) - r(0)}{r(\pi)} = \frac{r(AP) - r(P)}{r(AP)} , \quad (14)$$

since the resistance $R(\Theta)$ is defined as

$$R(\Theta) = r(\Theta)/A_0 , \quad (15)$$

where A_0 is the unit area. In a similar manner for the present non-collinear configurations, the difference in sheet resistances is given by

$$\Delta r(\Theta) = r(\Theta) - r(0) , \quad (16)$$

and the corresponding magnetoresistance by

$$MR(\Theta) = \frac{\Delta r(\Theta)}{r(\Theta)} . \quad (17)$$

The difference in sheet resistances can again be expanded in a power series in $\cos \Theta$

$$\Delta r(\Theta) = \alpha(1 - \cos(\Theta)) + \beta \cos^2(\Theta) + \gamma \cos^3(\Theta) + \dots , \quad (18)$$

with $\alpha = r(\pi/2) - r(0)$. It will be shown later on that in most of the cases investigated in here

$$\Delta r(\Theta) \sim \Delta r^{(1)}(\Theta) = \alpha(1 - \cos(\Theta)) , \quad (19)$$

i.e.,

$$r(\Theta) = r(0) + \alpha(1 - \cos(\Theta)) . \quad (20)$$

C. Magnetic Joule's heat generated by a current

For $I = 0$, Θ takes on its equilibrium value Θ_{eq} . As the current I is turned on, the relative orientation of the two magnetic layers changes to Θ . Evidently, the work done to accomplish this rotation is $\Delta E(\Theta) = E(\Theta) - E(\Theta_{\text{eq}})$. Suppose that this energy difference is equal to the energy lost by the current in the form of a “magnetic” contribution to the Joule's heat Q ,

$$Q = R(\Theta)I^2 .$$

Thus for a fixed current I ,

$$\Delta E(\Theta) = \tau R(\Theta)I^2 ,$$

where τ is the time required to accomplish the rotation. This equation can be solved for the function $\Theta(I)$, whose inverse is given by

$$I(\Theta) = \pm \sqrt{A_0/\tau} \sqrt{r(\Theta)^{-1} \Delta E(\Theta)} , \quad (21)$$

where

$$\Delta E(\Theta) = E(\Theta) - E(0) + \min [\Delta E(\Theta)] , \quad (22)$$

i.e., where $\Delta E(\Theta)$ is a positive definite excitation energy.

Since Q , $\Delta E(\Theta)$ and therefore $I(\Theta)$ are scalar positive definite quantities, the above construction is independent of the direction of the current flow. Nevertheless, in the following, the concept of twisting energies $\Delta E(\Theta)$ and the corresponding magnetic Joule's heat generated during a time interval τ shall be used to explore the physics of current induced switching. In short, evidence will be provided that the origin of the work done against the exchange forces acting between the two magnetic layers is the magnetic contribution to the energy dissipation from the current.

It might seem that by using an energy flux relation the problem of evaluating the current I was only shifted to yet another unknown quantity, namely to the characteristic time τ , whose theoretical description and evaluation therefore has to be the subject of the next few sections. Furthermore, it has to be pointed out that any comparison with experimental data

has to take into account also the actual area A_0 present in a given experiment. However, before going ahead to discuss these two quantities, the computational details of the ab-initio related parts of this paper shall be given.

D. Computational details

The effective scattering potentials and exchange fields of spin valve systems of the type fcc-Co(100)/Co₁₂/Cu_{*n*}/Co_{*m*}/Co(100), $12 \leq n \leq 36$, $m \geq 11$ were determined selfconsistently using the fully relativistic spin-polarized Screened Korringa-Kohn-Rostoker method,²⁶ where at least m layers of Co served as "buffer" to the semi-infinite leads. It should be noted that because of the special features of the applied screened structure constants²⁶ the total number of atomic layers between the two semi-infinite systems has to be a multiple of three. For this reason the thickness of the right buffer had to be kept variable. In all cases the local density approximation of Vosko et al.²⁹ and, in order to obtain selfconsistency, a total of 45 k_{\parallel} points in the irreducible part of the surface Brillouin zone (IBZ) was applied. All selfconsistent calculations were performed with the orientation of the magnetization pointing uniformly perpendicular to the planes of atoms (reference configuration).

In using the magnetic force theorem the twisting energies with respect to this reference configuration were then evaluated for each n using the symmetric arrangement, i.e., for the left half of the system (fcc-Co(100)/Co₁₂/Cu_{*n*/2}) the orientation of the magnetization remained unchanged whereas the right half was rotated by a particular (uniform) angle Θ . For this kind of calculation a total of 960 k_{\parallel} points in the IBZ was used, a set-up, which yields very reliable results. For further computational details concerning the Screened Korringa-Kohn-Rostoker method and the evaluation of band energies, see the review article in Ref. 26.

The sheet resistances for a given rotation angle Θ were first evaluated by means of the fully relativistic version of the Kubo-Greenwood equation at $E_F + i\delta$, $\delta > 0$, and then numerically continued to the real energy axis. In this part of the calculations for the occurring Brillouin zone integrals a total of 1830 k_{\parallel} points was used. For a detailed discussion of this approach, see the review article in Ref. 27.

III. THE LANDAU–LIFSHITZ–GILBERT EQUATION

From the polar form of the Landau-Lifshitz-Gilbert (LLG) equation,³⁰

$$\frac{d\vec{\mathcal{M}}}{dt} = \frac{\gamma_G}{1 + \alpha_G^2} \left[-\vec{\mathcal{M}} \times \vec{H}^{\text{eff}} + \frac{\alpha_G}{\mathcal{M}_0} \vec{\mathcal{M}} \times (\vec{\mathcal{M}} \times \vec{H}^{\text{eff}}) \right], \quad (\gamma_G, \alpha_G > 0), \quad (23)$$

where γ_G is the Gilbert gyromagnetic ratio (precession constant), α_G is the dimensionless Gilbert damping parameter, $\vec{\mathcal{M}}$ is the magnetization, $\mathcal{M}_0 = |\vec{\mathcal{M}}|$, and \vec{H}^{eff} is the local and time-dependent effective field, one immediately observes that (1) $\vec{\mathcal{M}}$ precesses almost purely, if damping is low ($\alpha_G \rightarrow 0$),³¹ (2) almost no precession, but slow switching occurs, when the damping is high ($\alpha_G \rightarrow \infty$)³², and (3) the fastest switching refers to $\alpha_G = 1$.³³ Rewriting the LLG equation in terms of an experimental damping parameter G ,³⁴

$$\frac{1}{\gamma_G} \frac{d\vec{\mathcal{M}}}{dt} = -\vec{\mathcal{M}} \times \vec{H}^{\text{eff}} + \frac{G}{\gamma_G^2 \mathcal{M}_0^2} \left(\vec{\mathcal{M}} \times \frac{d\vec{\mathcal{M}}}{dt} \right), \quad (24)$$

the dimensionless Gilbert parameter α_G is given by³⁵

$$\alpha_G = \frac{G}{\gamma_G \mathcal{M}_0}, \quad (25)$$

and the Gilbert gyromagnetic ratio γ_G by^{17,31,36,37}

$$\gamma_G = \frac{g\mu_B}{\hbar} = \frac{g|e|}{2m_e}, \quad (26)$$

where e refers to the elementary charge, m_e to the mass of an electron, μ_B to the Bohr magneton, and g is the (electronic) Landé-factor. Experimentally,^{35,38} it has been shown that in multilayer systems G in Eq. (25) varies linearly with $1/d$, where d is the film thickness, see also Tab. I.

By definition the magnetization $\vec{\mathcal{M}}$ refers to the volume averaged total magnetic moment. Assuming, however, that in a layered system the layer-resolved magnetic moments \vec{M}_i , where i denotes atomic layers, are coherently precessing,³⁹ it is sufficient to describe the magnetization dynamics of the layered system in terms of the motion of either the layer averaged magnetic moment \vec{M} ,

$$\frac{d\vec{M}}{dt} = -\gamma \vec{M} \times \vec{H}^{\text{eff}} + \alpha \frac{\vec{M}}{M_0} \times (\vec{M} \times \vec{H}^{\text{eff}}), \quad (27)$$

$$\vec{M} = \frac{1}{N} \sum_{i=1}^N \vec{M}_i,$$

where N denotes the number of magnetic layers, e.g. $N = m + n/2$, or in terms of the magnetization direction \vec{n} :^{30,40}

$$\frac{d\vec{n}}{dt} = -\gamma \vec{n} \times \vec{H}^{\text{eff}} + \alpha \vec{n} \times \left(\vec{n} \times \vec{H}^{\text{eff}} \right) , \quad \vec{n} = \frac{\vec{M}}{M_0} . \quad (28)$$

It should be noted that the equivalence of these two equations, namely Eqs. (27) and (28), relies on the conservation of \mathcal{M} , which in turn implies that $|\vec{M}| = M_0$ and $|\vec{n}| = 1$.

A. Internal effective field

The local effective field \vec{H}^{eff} that enters Eqs. (27) and (28) can directly be derived from the Helmholtz free energy density by taking its variational derivative with respect to the magnetization,^{33,35,36,41}

$$\vec{H}^{\text{eff}} = -\frac{\partial \mathcal{F}}{\partial \vec{\mathcal{M}}} = -\nabla_{\vec{\mathcal{M}}} \mathcal{F} , \quad \text{with} \quad \mathcal{F} = \frac{F}{V} \quad (29)$$

where V is the total characteristic volume of the system and the free energy F includes the exchange energy, the crystalline anisotropy energy, external magnetic fields, etc.,^{40,42} either in a parameter-free manner or by using different types of model Hamiltonians. Since for layered systems as considered in here,

$$\nabla_{\vec{\mathcal{M}}} = \Omega_0 \sum_{\mu=x,y,z} \vec{e}_\mu \frac{\partial}{\partial M_\mu} = \Omega_0 \nabla_{\vec{M}} ,$$

Eq. (29) can be written as

$$\vec{H}^{\text{eff}} = \frac{\partial \overline{F}}{\partial \vec{M}} = -\nabla_{\vec{M}} \overline{F} , \quad (30)$$

where the Helmholtz free energy \overline{F} ,

$$\overline{F} = \frac{1}{N} \sum_{i=1}^N F_i ,$$

refers to the reference volume Ω_0 and N is again the number of magnetic layers considered.

According to Eq. (30) the internal effective field, \vec{H}^{E} , arises from the contribution of the total energy E_b to the free energy,

$$\vec{H}^{\text{E}} = -\frac{\partial E_b}{\partial \vec{M}} = -\nabla_{\vec{M}} E_b .$$

Assuming, e.g., in terms of Eq.(8) that the derivatives

$$\frac{\partial^k E_b(\vec{M}_0)}{\partial M_x^{k_1} \partial M_y^{k_2} \partial M_z^{k_3}} , \quad \sum_{j=1}^3 k_j = k = 1, \dots, n \quad (k_j, k, n \in \mathbb{N}) ,$$

in the below Taylor series expansion of the total energy,

$$E_b(\vec{M}_0 + \vec{M}) \simeq E_b(\vec{M}_0) + \sum_{k=1}^p \frac{1}{k!} \left(\vec{M} \cdot \nabla_{\vec{M}} \right)^k E_b(\vec{M}_0) , \quad (31)$$

are available up to a certain order p , where \vec{M}_0 is the initial reference moment, the Cartesian components of the internal effective field can directly be given.

In particular, if the change in the moment \vec{M} is constrained to the 0yz-plane,

$$\vec{M} = M_y \vec{e}_y + M_z \vec{e}_z , \quad (M_x = 0) ,$$

then

$$\vec{H}^E = - \sum_{k=1}^p \sum_{q=0}^k \frac{\partial^k E(\vec{M}_0)}{\partial M_y^{k-q} \partial M_z^q} \left[\frac{M_y^{k-q-1} M_z^q}{(k-q-1)! q!} \vec{e}_y + \frac{M_y^{k-q} M_z^{q-1}}{(k-q)! (q-1)!} \vec{e}_z \right] , \quad (32)$$

with $\vec{M}_0 = M_0 \vec{e}_z$ being the initial, ground state moment. Provided that the magnitude of the moment is preserved,

$$M_0^2 = M_y^2 + M_z^2 = M^2 , \quad (33)$$

by keeping in Eq. (31) only terms up $p = 3$, one gets

$$\Delta E_b(\vec{M}) = E_b(\vec{M}_0 + \vec{M}) - E_b(\vec{M}_0) \simeq a - a \frac{M_z}{M_0} + b \frac{M_z^2}{M_0^2} + c \frac{M_z^3}{M_0^3} , \quad (34)$$

where the coefficients a , b and c are defined in Eqs. (9) and (13). Therefore the energy torque rotating the moment is given by

$$\vec{M} \times \vec{H}^E = \vec{e}_x M_y H_z^E = -n_y (-a + 2b n_z + 3c n_z^2) \vec{e}_x , \quad (35)$$

whereas

$$\vec{M} \times (\vec{M} \times \vec{H}^E) = -n_y (-a + 2b n_z + 3c n_z^2) (M_z \vec{e}_y - M_y \vec{e}_z) . \quad (36)$$

B. The characteristic time of switching

Inserting the internal effective field \vec{H}^E into the LLG equation (in the absence of precession around the z-axis),

$$\frac{d\vec{M}}{dt} \simeq \alpha \frac{\vec{M}}{M_0} \times (\vec{M} \times \vec{H}^E) , \quad \alpha = \alpha_G \frac{\gamma_G}{1 + \alpha_G^2} ,$$

then leads to

$$M_0 \frac{dn_x}{dt} = 0 , \quad (37)$$

$$M_0 \frac{dn_y}{dt} = -\alpha n_y n_z (-a + 2b n_z + 3c n_z^2) , \quad (38)$$

$$M_0 \frac{dn_z}{dt} = \alpha n_y^2 (-a + 2b n_z + 3c n_z^2) . \quad (39)$$

Since according to Eq. (33), $n_y^2 + n_z^2 = 1$, Eq. (39) reduces to

$$M_0 \frac{dn_z}{dt} = \alpha (1 - n_z^2) (-a + 2b n_z + 3c n_z^2) . \quad (40)$$

Assuming that $n_z \neq \pm 1$ or $(-b \pm \sqrt{b^2 + 3ac}) / 3c$ and $b^2 + 3ac > 0$, $c \neq 0$, Eq. (40) can directly be integrated and leads to the time $\tau = t_f - t_i$ needed to change n_z from $n_z^i = n_z(t_i)$ to $n_z^f = n_z(t_f)$

$$\begin{aligned} \frac{\alpha}{M_0} \tau = & \frac{1}{2[(3c-a)-2b]} \ln \left| \frac{n_z^f + 1}{n_z^i + 1} \right| - \frac{1}{2[(3c-a)+2b]} \ln \left| \frac{n_z^f - 1}{n_z^i - 1} \right| \\ & - \frac{b}{(3c-a)^2 - 4b^2} \ln \left| \frac{3c(n_z^f)^2 + 2b n_z^f - a}{3c(n_z^i)^2 + 2b n_z^i - a} \right| \\ & + \frac{1}{(3c-a)^2 - 4b^2} \frac{a(3c-a) + 2b^2}{2\sqrt{b^2 + 3ac}} \\ & \times \ln \left| \frac{(b + 3c n_z^f) - \sqrt{b^2 + 3ac}}{(b + 3c n_z^i) - \sqrt{b^2 + 3ac}} \frac{(b + 3c n_z^i) + \sqrt{b^2 + 3ac}}{(b + 3c n_z^f) + \sqrt{b^2 + 3ac}} \right| . \end{aligned} \quad (41)$$

Thus the time $\tau(\alpha_G)$ needed to change n_z from n_z^i to n_z^f as a function of the Gilbert damping parameter $\alpha_G > 0$, when using $\alpha = \alpha_G \gamma_G / (1 + \alpha_G^2)$ and Eq. (26), can be written as

$$\tau(\alpha_G) = C \frac{M_0}{\gamma_G} \frac{1 + \alpha_G^2}{\alpha_G} = \hbar \frac{\mathfrak{M}_0}{g} C \frac{1 + \alpha_G^2}{\alpha_G} , \quad (42)$$

where C denotes the rhs of Eq. (41) and \mathfrak{M}_0 is the magnetic moment M_0 in units of Bohr magnetons μ_B .

According to Eq. (42) it follows that the minimal time of changing n_z from n_z^i to n_z^f is given by

$$\tau_{\min} = \tau(\alpha_G = 1) = 2\hbar \frac{\mathfrak{M}_0}{g} C \quad \text{and} \quad \tau(\alpha_G) = \frac{1 + \alpha_G^2}{\alpha_G} \frac{\tau_{\min}}{2} . \quad (43)$$

IV. RESULTS

A. Magnetization and switching times

The selfconsistently obtained constant magnitude of the magnetization for fcc Co/Cu/Co(100) and in the case of a thin Co slab of $M_0^{\text{fcc Co}} = 1.418 \times 10^6 \text{ A m}^{-1}$ is in very good agreement with the available experimental data for Co bulk, see Ref. 43 or 44. By using the experimental Landé g-factor for fcc Co, namely $g^{\text{fcc Co}} = 2.146 \pm 0.02$,⁴⁵ $\gamma_G^{\text{fcc Co}} = 18.87213449 \times 10^{10} \text{ m A}^{-1} \text{ s}^{-1}$, which in turn yields the below ratio

$$\frac{M_0^{\text{fcc Co}}}{\gamma_G^{\text{fcc Co}}} = \hbar \frac{\mathfrak{M}_0^{\text{fcc Co}}}{g^{\text{fcc Co}}} = 0.782531193 \times 10^{-34} \text{ Js} = 4.884173446 \times 10^{-16} \text{ eVs} .$$

Since according to Tab. II the quantities on the rhs of Eq. (41) are of the order of $(\text{meV})^{-1} = 10^3 (\text{eV})^{-1}$, this implies that the time needed to change the moment direction from n_z^i to n_z^f is of the order of 10^{-13} s , namely femtoseconds. From Tab. III one immediately can see that the theoretically obtained values of τ_{\min} are within the range of values known from micromagnetic simulations for a polycrystalline thin Co film, which showed that the reversal time ranges from 0.05 ns for $\alpha_G = 1$ to 0.2 ns for $\alpha_G = 0.1$.⁴³ It should be noted that because the sign of τ_{\min} is uniquely determined by the sign of the initial and final values for n_z , in Tab. III only those values for n_z^i and n_z^f are listed, which yield $\tau_{\min} > 0$. The sign of the such determined n_z^f confirms therefore independently the ground state configuration predicted by the magnetic force theorem, see Eq. (7).

As can be seen from the corresponding column in Tab. III the switching time is largest for the Gilbert damping parameter of Co bulk. By scaling α_G to the thickness of the thin (rotated) Co slab used in the present calculations according to values found for Co_N/Cu/Co(100),⁴⁴ the magnetization reversal time $\tau(\alpha_G)$ in Eq. (43) changes only very moderately in comparison with τ_{\min} .

B. The importance of cross sections (unit areas)

Going now back to Eq. (21), rewritten below by indicating the appropriate units,

$$I(\Theta)|_{\text{SI}} = \pm 1.265771437 \cdot \sqrt{\frac{\langle A_0 \rangle_{\text{SI}}}{\langle \tau \rangle_{\text{SI}}}} \sqrt{\frac{\langle \Delta E(\Theta) \rangle_{\text{meV}}}{\langle r(\Theta) \rangle_{\text{m}\Omega \cdot \mu\text{m}^2}}} \text{ mA} , \quad (44)$$

it is obvious that for any kind of comparison to experiment not only τ has to be evaluated, but also that A_0 , the surface perpendicular to the z axis through which the current $I(\Theta)$ flows, has to be taken into account. Usually the cross section of nanopillars is given in nanometer (nm), i.e., is of the order of

$$\langle A_0 \rangle_{\text{SI}} = \langle A_0 \rangle_{\text{nm}^2} \times 10^{-18} ,$$

which combined with the switching time (in nanoseconds),

$$\langle \tau \rangle_{\text{SI}} = \langle \tau \rangle_{\text{ns}} \times 10^{-9} ,$$

yields the following factor that multiplies the square root of the (quantum mechanically derived) quotient of twisting energy and sheet resistance in Eq. (44),

$$\sqrt{\frac{\langle A_0 \rangle_{\text{SI}}}{\langle \tau \rangle_{\text{SI}}}} = \sqrt{\frac{\langle A_0 \rangle_{\text{nm}^2} \times 10^{-18}}{\langle \tau \rangle_{\text{ns}} \times 10^{-9}}} = \sqrt{\frac{\langle A_0 \rangle_{\text{nm}^2}}{\langle \tau \rangle_{\text{ns}}}} \times 10^{-9} .$$

In using, e.g., $\langle A_0 \rangle_{\text{nm}^2} = 120000^{12}$, other values of $\langle A_0 \rangle_{\text{nm}^2}$ are listed in Tab. IV, and $\langle \tau_{\text{min}} \rangle_{\text{ns}} = 0.01$, this results into a value for $\sqrt{\langle A_0 \rangle_{\text{SI}} / \langle \tau_{\text{min}} \rangle_{\text{SI}}}$ of about 0.11.

C. Twisting energies and currents

In all figures showing twisting energies and sheet resistances, etc., the actually calculated values are displayed, solid lines only serve as guidance to the eye. For illustrative purposes also the first order approximation to the twisting energy is depicted in these figures as a dashed line. As it is not possible to show all results obtained these figures concentrate on systems with the spacer thickness varying between about 35 - 50 Å. This still results in a considerable number of figures, which, however, seems to be necessary considering that in experimental studies mostly nanopillars are used, i.e., most likely an average over thicknesses is recorded, and also in order to illustrate the complexity of the effects to be seen. Furthermore, in all figures for the current $I(\Theta)$ the factor $\sqrt{\langle A_0 \rangle_{\text{SI}} / \langle \tau_{\text{min}} \rangle_{\text{SI}}}$ in Eq. (44) is replaced by unity.

In the investigated range of spacer thicknesses the number of cases in which the twisting energy is proportional to $(1 - \cos(\Theta))$, see the corresponding figures for $n \geq 31$, is surprisingly small, whereas in all cases the sheet resistance – more or less – is of this shape. This in turn implies that all special features to be seen for $I(\Theta)$ are mostly related to the functional

form of the twisting energy. Taking for example $n = 20$, $I(\Theta)$ remains about constant for $\Theta \geq 90^\circ$, a value which refers also to the critical current that has to be applied to drive the system from parallel to antiparallel. However, one also can see from this figure that $\Delta E_b(\Theta)$ has a maximum at about 140° : the system has to overcome a small barrier to return to the ground state (parallel configuration). From the entry showing the magnetoresistance versus current, it is evident that at the critical current the magnetoresistance jumps by about 20%. For $n = 21$ the situation is even more dramatic, since $\Delta E_b(\Theta)$ has quite a large maximum at 90° , the AP configuration being only slightly less energetically favored than the P configuration. In this particular system the meaning of the critical current is quite obvious: it simply is the maximum in the $I(\Theta)$ versus Θ curve. The same situation, even more impressive, pertains for $n = 25$, since now the parallel and antiparallel configuration are virtually degenerated in energy, separated, however, by quite a barrier. The figures for $n = 20, 21, 23, 24, 25$ and 27 are perfect ab-initio analoga for the schematic effective two-level energy diagram mentioned in the introduction: the energy displayed in this *ad hoc* scheme is nothing but the twisting energy, the schematic abscises being the relative angle between the two orientations of the magnetization.

The system with 26 Cu spacer layers is in particular interesting, since a non-collinear configuration is the ground state. In this case a tiny current (about 0.05 mA in this figure) produces a magnetoresistance that can be either zero, 1.5 or about 6 %. It should be noted that the energy barrier between the ground state and the parallel configuration is minute: the system can almost freely oscillate between magnetic configurations for values of $\Theta \leq 60^\circ$. Another interesting case seems to be for 30 Cu spacer layers, which shows a strong deviation from $\Delta E_b^{(1)}(\Theta)$ at about $\Theta = 90^\circ$, not enough, however, to cause an additional minimum between the AP (ground state) and the P configuration. For $0 \leq \Theta \leq 100^\circ$ the current $I(\Theta)$ varies almost linear, changes slope, and varies again almost linear for $\Theta > 100^\circ$.

For $n \geq 31$ no more interesting effects are observed: the twisting energy can be described very well in terms of $\Delta E_b^{(1)}(\Theta)$; in order to switch from parallel to antiparallel or vice versa a current of about 0.35 - 0.6 mA is needed. It should be recalled that all values of $I(\Theta)$ quoted in this section refer to $\sqrt{\langle A_0 \rangle_{\text{SI}} / \langle \tau_{\text{min}} \rangle_{\text{SI}}} = 1$ in Eq. (44).

In the last figure finally the rotation of the magnetization around the z-axis (precession) is shown for $n = 25$. As can be seen the precessional changes in the twisting energy are very small indeed. This figure justifies *a posteriori* the approach taken to evaluate and discuss the

switching time τ_{\min} .

V. DISCUSSION

In viewing now all the various cases discussed above the following observations can be added: (1) if the slope of the magnetoresistance with respect to the current is uniformly positive (negative), the parallel (antiparallel) magnetic configuration is favoured (see, $n = 31, 33$ versus $n = 32$), (2) if it becomes approximately infinite at a certain current then a jump in the magnetoresistance occurs (e.g., $n = 20, 24, 28$), and (3) if this slope changes sign, a more complicated behavior pertains (e.g., $n = 21, 22, 25, 26$). In the latter case the system either remains in the switched configuration ($n = 21, 25$) or because of a non-collinear ground state oscillations in the magnetoresistance between zero and a few percent can occur when a very small current is applied ($n = 26$). The so-called telegraph noise seems to refer to the jumping between such minima in the twisting energy, the jumping rates obviously being connected with the barrier between these minima. The current needed to switch a configuration from parallel to antiparallel (or vice versa) refers to the largest value of $I(\Theta)$.

The present results suggest that the efficiency of current-driven switching can considerably be optimized by varying the spacer thickness: theoretically in using a spacer thickness of about 43 Å (25 layers of Cu) perfect switching can be achieved such that the system remains in the switched state after the current is turned off. Further theoretical investigations using the approach presented in here can include interdiffusion effects at interfaces or refer to different kinds of magnetic slabs (leads) such as for example permalloy, a system, which because of anisotropy effects in the magnetoresistance perhaps is even more complicated than the present Co/Cu/Co trilayer.

Altogether correlating the twisting energy and the corresponding resistance with the current yields a very consistent view of the complexity found in current-driven experiments. Clearly enough this correlation suffers from the fact that up-to-now no quantum mechanical description for the Gilbert damping factor was found and that a linear response theory (Kubo-Greenwood equation) is used to evaluate the electric transport properties, i.e., that the current had to be formulated as a scalar quantity.

Finally, it has to be remarked that the experimentally observed critical switching currents are by a factor of about 10 - 100 larger than the ones obtained in here. It has to

be remembered, however, that in here an ideal Co/Cu/Co trilayer was assumed while most experiments are based on rather complicated nanostructures such as for example nanopillars and therefore - although a consistent approach to was introduced in order to evaluate switching times in terms of ab-initio parameters - also the question of a comparable cross section (unit area) is of quite some importance.

VI. ACKNOWLEDGEMENT

The authors are grateful for many fruitful discussions with Profs. P. M. Levy, J. Bass and C. Sommers. This work has been financed by the Center for Computational Materials Science (Contract No. GZ 45.531), a special grant from the Technical University of Vienna, and the Hungarian National Scientific Research Foundation (Contracts OTKA T037856 and OTKA T046267).

-
- ¹ M. Tsoi, A. G. M. Jansen, J. Bass, W.-C. Chiang, M. Seck, V. Tsoi, and P. Wyder, Phys. Rev. Lett. **19**, 4281 (1998).
 - ² J. Z. Sun, J. Mag. Magn. Mat. **202**, 157 (1999).
 - ³ J.-E. Wegrowe, D. Kelly, Y. Jaccard, Ph. Guittienne, and J.-Ph. Ansermet, Europhys. Lett. **45**, 626 (1999).
 - ⁴ F. J. Albert, J. A. Kantine, R. A. Buhrman, and D. C. Ralph, Appl. Phys. Lett. **77**, 3809 (2000).
 - ⁵ J. A. Katine, F. J. Albert, R. A. Buhrman, E. B. Myers, and D. C. Ralph, Phys. Rev. Letters **84**, 3149 (2000).
 - ⁶ J. Grollier, D. Lacour, V. Cros, A. Hamzić, A. Vaurès, A. Fert, D. Adam, and G. Faini, J. Appl. Phys. **92**, 4825 (2002).
 - ⁷ F. J. Albert, N. C. Emley, E. B. Myers, D. C. Ralph, and R. A. Buhrman, Phys. Rev. Lett. **89**, 226802 (2002).
 - ⁸ S. Urazhdin, N. O. Birge, W. P. Pratt Jr., and J. Bass, Phys. Rev. Lett. **91**, 146803 (2003).
 - ⁹ S. Urazhdin, H. Kurt, W. P. Pratt Jr., and J. Bass, Appl. Phys. Lett. **83**, 114 (2003).
 - ¹⁰ J. Grollier, P. Boulenc, V. Cros, A. Hamzić, A. Vaurès, A. Fert, and G. Faini, Appl. Phys. Lett. **83**, 509 (2003).
 - ¹¹ S. I. Kiselev, J. C. Sankey, I. N. Krivorotov, N. C. Emley, R. J. Schoelkopf, R. A. Buhrman and D. C. Ralph, Nature **425**, 380 (2003).
 - ¹² J. Grollier, V. Cros, H. Jaffrès, A. Hamzic, J. M. George, G. Faini, J. Ben Youssef, H. Le Gall, and A. Fert, Phys. Rev. B **67**, 174402 (2003).
 - ¹³ B. Özyilmaz, A. D. Kent, D. Monsma, J. Z. Sun, M. J. Rooks, and R. H. Koch, Phys. Rev. Lett. **91**, 67203 (2003).
 - ¹⁴ J. Bass, S. Urazhdin, N. O. Birge, and W. P. Pratt Jr., phys. stat. sol. (a), DOI 10.1002/pssa.200304421 (2004).
 - ¹⁵ J. C. Slonczewski, J. Mag. Magn. Mat. **159**, L1 (1996).
 - ¹⁶ L. Berger, Phys. Rev. B **54**, 9353 (1996).
 - ¹⁷ Y. B. Bazaliy, B. A. Jones, and S.-C. Zhang, Phys. Rev. B **57**, R3213 (1998).
 - ¹⁸ J. C. Slonszewski, J. Mag. Magn. Mat. **195**, L261 (1999).

- ¹⁹ A. Brataas, Yu. V. Nazarov, and G. E. W. Bauer, Phys. Rev. Lett. **84**, 2481 (2000).
- ²⁰ X. Waintal, E. B. Myers, P. W. Brouwer, and D. C. Ralph, Phys. Rev. B **62**, 12317 (2000).
- ²¹ J. Z. Sun, Phys. Rev. B **62**, 570 (2000).
- ²² C. Heide, P. E. Zilberman, and R. J. Elliot, Phys. Rev. B **63**, 066424 (2001).
- ²³ C. Heide, Phys. Rev. Lett. **87**, 197201 (2001).
- ²⁴ S. Zhang, P. M. Levy and A. Fert, Phys. Rev Lett. **88**, 236601 (2002).
- ²⁵ D. H. Hernando, Yu. V. Nazarov, A. Brataas, and G. E. W. Bauer, Phys. Rev. B **62**, 5700 (2002).
- ²⁶ L. Szunyogh, B. Újfalussy, P. Weinberger, and J. Kollár, Phys. Rev. B **49**, 2721 (1994); L. Szunyogh, B. Újfalussy, and P. Weinberger, Phys. Rev. B **51**, 9552 (1995); B. Újfalussy, L. Szunyogh, and P. Weinberger, Phys. Rev. B **51**, 12836 (1995); P. Weinberger and L. Szunyogh, Computational Materials Science **17**, 414 (2000).
- ²⁷ P. Weinberger, Physics Reports **377**, 281 - 387 (2003).
- ²⁸ H. J. F. Jansen, Phys. Rev. B **59**, 4699 (1999).
- ²⁹ S. H. Vosko, L. Wilk, and M. Nusair, Can. J. Phys. **58**, 1200 (1980).
- ³⁰ Y. Tserkovnyak, A. Brataas, and G. E. W. Bauer, Phys. Rev. Letters **88**, 117601 (2002).
- ³¹ L. D. Landau and E. M. Lifshitz, *Statistical Physics*, Vol. 9 of *Course of Theoretical Physics* (Pergamon Press, Oxford, 1999).
- ³² J. C. Mallinson, IEEE Transactions on Magnetism **23**, 2003 (1987).
- ³³ J. C. Mallinson, IEEE Transactions on Magnetism **36**, 1976 (2000).
- ³⁴ B. Heinrich, R. Urban, and G. Woltersdorf, IEEE Transactions on Magnetism **38**, 2496 (2002).
- ³⁵ B. Heinrich, G. Woltersdorf, R. Urban, and E. Simanek, J. Magn. Magn. Materials **258-259**, 376 (2003).
- ³⁶ C. J. Garcia-Cervera and E. Weinan, J. Appl. Physics **90**, 370 (2001).
- ³⁷ M. D. Stiles and A. Zangwill, Phys. Rev. B **66**, 014407 (2002).
- ³⁸ R. Urban, G. Woltersdorf, and B. Heinrich, Phys. Rev. Letters **87**, 217204 (2001).
- ³⁹ D. L. Mills, Phys. Rev. B **68**, 14419 (2003).
- ⁴⁰ G. Brown, M. A. Novotny, and P. A. Rikvold, J. Appl. Physics **93**, 6817 (2003).
- ⁴¹ J. Kunes and V. Kambersky, Phys. Rev. B **65**, 212411 (2002).
- ⁴² L. F. Alvarez, O. Pla, and O. Chubykalo, Phys. Rev. B **61**, 11 613 (2000).
- ⁴³ A. W. Spargo, P. H. W. Ridley, and G. W. Roberts, J. Magn. Magn. Materials **258-259**, 35

- (2003).
- ⁴⁴ E. B. Myers, D. C. Ralph, J. A. Katine, R. N. Louie, and R. A. Buhrman, *Science* **285**, 867 (1999).
 - ⁴⁵ F. Schreiber, J. Pflaum, Z. Frait, T. Muhge, and J. Pelzl, *Solid State Commun.* **93**, 965 (1995).
 - ⁴⁶ B. Heinrich, K. B. Urquhart, A. S. Arrott, J. F. Cochran, K. Myrtle, and S. T. Purcell, *Phys. Rev. Letters* **59**, 1756 (1987).
 - ⁴⁷ B. Heinrich, R. Urban, and G. Woltersdorf, *J. Appl. Physics* **91**, 7523 (2002).
 - ⁴⁸ J. Lindner, K. Lenz, E. Kosubek, K. Baberschke, D. Spoddig, R. Meckenstock, J. Pelzl, Z. Frait, and D. L. Mills, *Phys. Rev. B* **68**, 60102 (2003).
 - ⁴⁹ B. Heinrich, G. Woltersdorf, R. Urban, and E. Simanek, *J. Appl. Physics* **93**, 7545 (2003).
 - ⁵⁰ L. Berger, *J. Appl. Physics* **90**, 4632 (2001).
 - ⁵¹ E. B. Myers, F. J. Albert, J. C. Sankey, E. Bonet, R. A. Buhrman, and D. C. Ralph, *Phys. Rev. Lett.* **89**, 196801 (2001).
 - ⁵² J.-E. Wegrowe, X. Hoffer, Ph. Guittienne, A. Fábíán, L. Gravier, and J.-Ph. Ansermet, *J. Appl. Phys.* **91**, 6806 (2002).
 - ⁵³ A. Fábíán, C. Terrier, S. Serrano Guisan, X. Hoffer, M. Dubey, L. Gravier, and J.-Ph. Ansermet, *Phys. Rev. Lett.* **91**, 257209 (2003).
 - ⁵⁴ J.-E. Wegrowe, *Phys. Rev. B* **68**, 214414 (2003).
 - ⁵⁵ J. Z. Sun, D. Monsma, T. S. Kuan, M. J. Rooks, D. W. Abraham, B. Özyilmaz, and A. D. Kent, *J. Appl. Phys.* **93**, 6859 (2003).
 - ⁵⁶ M. Tsoi, J. Z. Sun, M. J. Rooks, R. H. Koch, and S. S. P. Parkin, *Phys. Rev. B* **69**, 100406(R) (2004).
 - ⁵⁷ R. H. Koch, J. A. Katine, and J. Z. Sun, *Phys. Rev. Lett.* **92**, 88302 (2004).

TABLE I: Experimental damping parameter G for different systems.

material	type of system	G (10^8 s^{-1})
Fe	bulk	$0.5^{34}, 0.58^{46}$
		$0.59 \pm 0.06; 0.572 \pm 0.04^{45}$
		$0.8^{47} \ 0.7 \pm 0.06^{45}$
Fe	single film	$1.5^{35,38}$
		1.3 ± 0.1^{47}
Fe / Ag(100)	$d_{\text{Fe}} = 40 \text{ \AA}$	0.66^{46}
	$d_{\text{Fe}} = 24 \text{ \AA}$	0.65^{46}
	$d_{\text{Fe}} = 7 \text{ \AA}$	2.3^{46}
	$d_{\text{Fe}} = 4 \text{ \AA}$	5.7^{46}
Fe ₄ / V ₄		1.25^{48}
Fe ₄ / V ₂		0.90^{48}
Ni	bulk	$2.4^{34,47}$
Cu / Co(111)		1.4^{49}
Co / Cu(001)	fcc	3.0^{45}
Co	fcc, hard	2.8 ± 0.3^{45}
	easy direction	1.7 ± 0.2^{45}
Fe[001]	bcc	$0.0(63)^{41}$
Ni[001]	fcc	$0.(54)^{41}$
Ni[111]	fcc	$0.(45)^{41}$
Co[0001]	hcp	$0.0(36)^{41}$

TABLE II: Third order Taylor series expansion coefficients of the total energy in case of Co/Cu_n/Co. Notice that $b^2 + 3ac > 0$ and $(3c - a)^2 - 4b^2$ (not given here) are the smallest in magnitude for $n = 30$, see Eq. (41).

n	a (meV)	b (meV)	c (meV)
20	0.18482	1.21031	1.34444
21	0.10742	0.38908	0.57940
22	-0.01466	-0.46855	-0.34401
23	0.05495	0.33396	0.38826
24	-0.01887	-0.21263	-0.19021
25	0.09246	0.30579	0.49206
26	0.06293	0.65673	0.56195
27	-0.05575	-1.03111	-0.78382
28	0.21518	1.54457	1.64362
29	-0.01959	-0.25292	-0.20745
30	-0.02395	-0.17970	-0.12111
31	0.20914	1.64070	1.60557
32	-0.24502	-1.92659	-1.93901
33	0.17413	1.22408	1.28963

TABLE III: Switching times (ns) as obtained by using the third order Taylor series expansion coefficients of the total energy, see Tab. II for Co/Cu_n/Co_m. FS (P or AP) denotes the final magnetic configuration by assuming that for the thick Co slab the direction of the moment is $n_z^{(I)} = +1$.

n	m	n_z^i	n_z^f	FS	τ_{\min}	$\tau(\alpha_G^{\text{bulk}})^{30}$	$\tau(\alpha_G^{\text{Co/Cu/Co}})^{50}$	$\tau(\alpha_G^{\text{scaled}})^{44}$
20	13	-1	+1	P	0.01340	1.33999	0.54039	0.108 24
21	12	-1	+1	P	0.02506	2.50591	1.01058	0.186 97
22	14	+1	-1	AP	0.18977	18.97722	7.65309	1. 649 90
23	13	-1	+1	P	0.04415	4.41567	1.78074	0.356 67
24	12	+1	-1	AP	0.13645	13.64524	5.50282	1. 018 10
25	14	-1	+1	P = AP	0.02841	2.84111	1.14576	0.247 01
26	13	-1	+1	P \simeq GS	0.05414	5.41415	2.18341	0.437 33
27	12	+1	-1	AP	0.06667	6.66771	2.68894	0.497 49
28	11	-1	+1	P	0.01154	1.15445	0.46556	0.07902
29	13	+1	-1	AP	0.16889	16.88991	6.81132	1. 364 30
30	12	-1	+1	P (AP)	0.68836	68.83831	27.76096	5. 136 10
31	14	-1	+1	P	0.01358	1.35829	0.54777	0.118 09
32	13	+1	-1	AP	0.01064	1.06400	0.42909	0.08 594
33	12	-1	+1	P	0.01498	1.49796	0.60409	0.111 76

TABLE IV: Cross section of multilayer pillar sequence Co/Cu/Co used in experiments.

multilayer pillar sequence	cross section	A_0 (nm ²)
Co(100 nm)/Cu(4 nm)/Co(d_{Co}),	$5 \div 10$ nm diameter	$(1 \div 4) \cdot 19.63$
$d_{\text{Co}} = 2, 4, 7, 10$ nm ⁴⁴		
Co(100 Å)/Cu(60 Å)/Co(25 Å) ⁵	130 ± 30 nm diameter	$7853.98 \div 20106.19$
Co(40 nm)/Cu(6 nm)/Co(3 nm) ⁵¹	$\sim 50 \times 50$ nm (sample 1)	2500.00
	$\sim 130 \times 60$ nm (sample 2)	7800.00
Co(t_{Fixed} nm)/Cu(d_{Cu} nm)/Co(t_{Free} nm)	≤ 100 nm diameter	7853.98
$t_{\text{Fixed}} \geq 4t_{\text{Free}}$ ⁷		
Co(30 nm)/Cu(10 nm)/Co(10 nm) ⁵²	$\sim 60 \div 80$ nm diameter	$2827.43 \div 5026.55$
Co(15 nm)/Cu(10 nm)/Co(2.5 nm) ¹²	200×600 nm ²	120000.00
Co(10 nm)/Cu(10 nm)/Co(30 nm) ⁵³	~ 40 nm diameter	1256.64
Co(3 nm)/Cu(10 nm)/Co(12 nm) ¹³	~ 100 nm diameter	7853.98
Co(10 nm)/Cu(10 nm)/Co(30 nm) ⁵⁴	~ 40 nm diameter	1256.64
Co(3 nm)/Cu(10 nm)/Co(12 nm) ⁵⁵	0.05×0.10 μm ²	5000.00
	0.05×0.20 μm ²	10000.00
	0.07×0.14 μm ²	9800.00
	0.08×0.16 μm ²	12800.00
Co(3 nm)/Cu(10 nm)/Co(12 nm) ⁵⁶	$50 \div 200$ nm circumference	$198.94 \div 3183.10$
Co/Cu/Co(30 Å) ⁵⁷	0.05×0.10 μm ²	5000.00

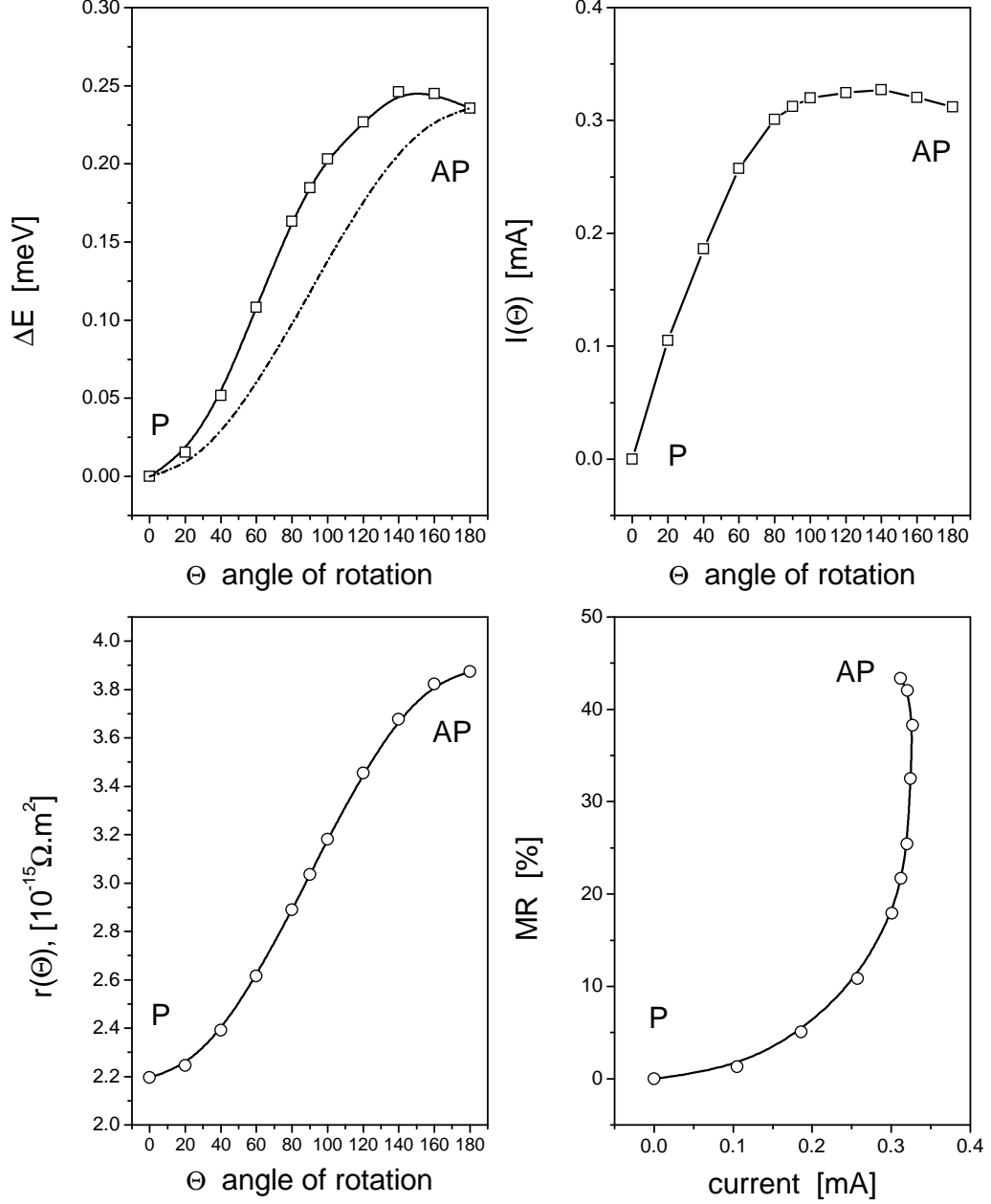


FIG. 1: Co/Cu₂₀/Co, spacer thickness: 34.65 Å. Left column: twisting energy and sheet resistance as a function of the rotation angle Θ . The dashed-dotted line refers to the first order approximation for the twisting energy. Right column: current as a function of the rotation angle Θ (top) and magnetoresistance as a function of the current (bottom), $\sqrt{\langle A_0 \rangle_{SI} / \langle \tau_{min} \rangle_{SI}} = 1$, see Eq.(44). Solid lines serve as guidance for the eye.

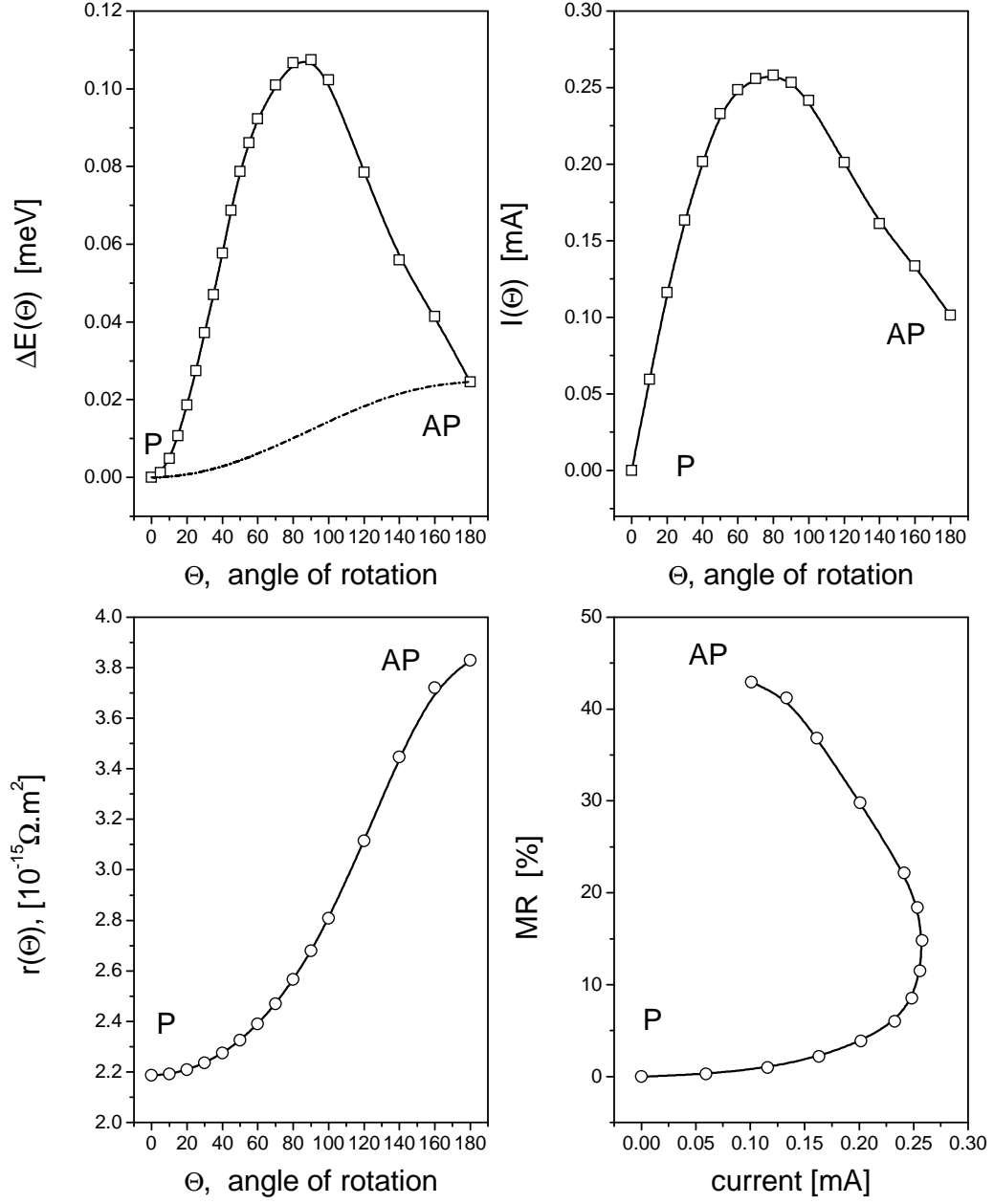


FIG. 2: Co/Cu₂₁/Co, spacer thickness: 36.39 Å. Left column: twisting energy and sheet resistance as a function of the rotation angle Θ . The dashed-dotted line refers to the first order approximation for the twisting energy. Right column: current as a function of the rotation angle Θ (top) and magnetoresistance as a function of the current (bottom), $\sqrt{\langle A_0 \rangle_{\text{SI}} / \langle \tau_{\text{min}} \rangle_{\text{SI}}} = 1$, see Eq.(44). Solid lines serve as guidance for the eye.

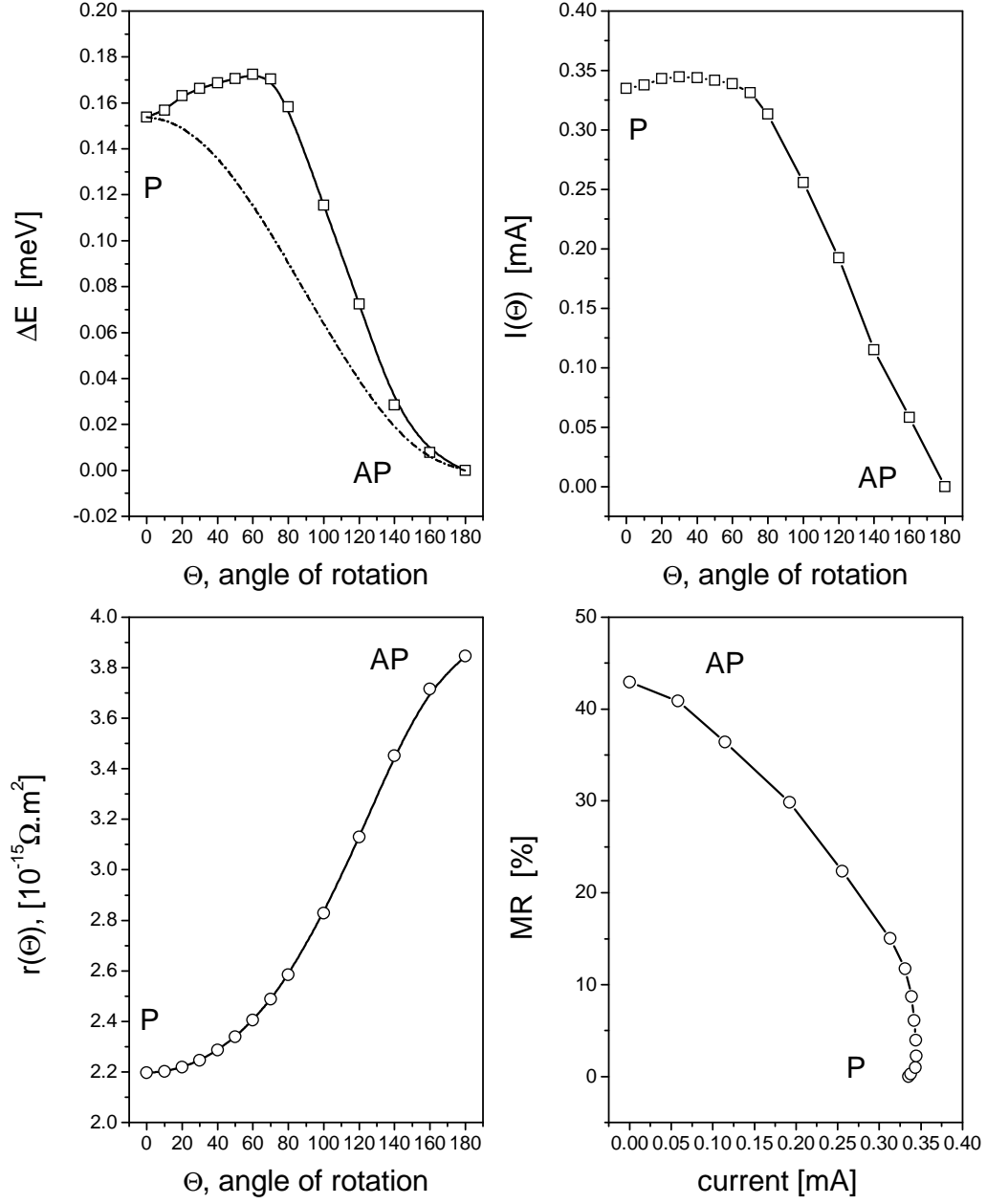


FIG. 3: Co/Cu₂₂/Co, spacer thickness: 38.12 Å. Left column: twisting energy and sheet resistance as a function of the rotation angle Θ . The dashed-dotted line refers to the first order approximation for the twisting energy. Right column: current as a function of the rotation angle Θ (top) and magnetoresistance as a function of the current (bottom), $\sqrt{\langle A_0 \rangle_{\text{SI}} / \langle \tau_{\text{min}} \rangle_{\text{SI}}} = 1$, see Eq.(44). Solid lines serve as guidance for the eye.

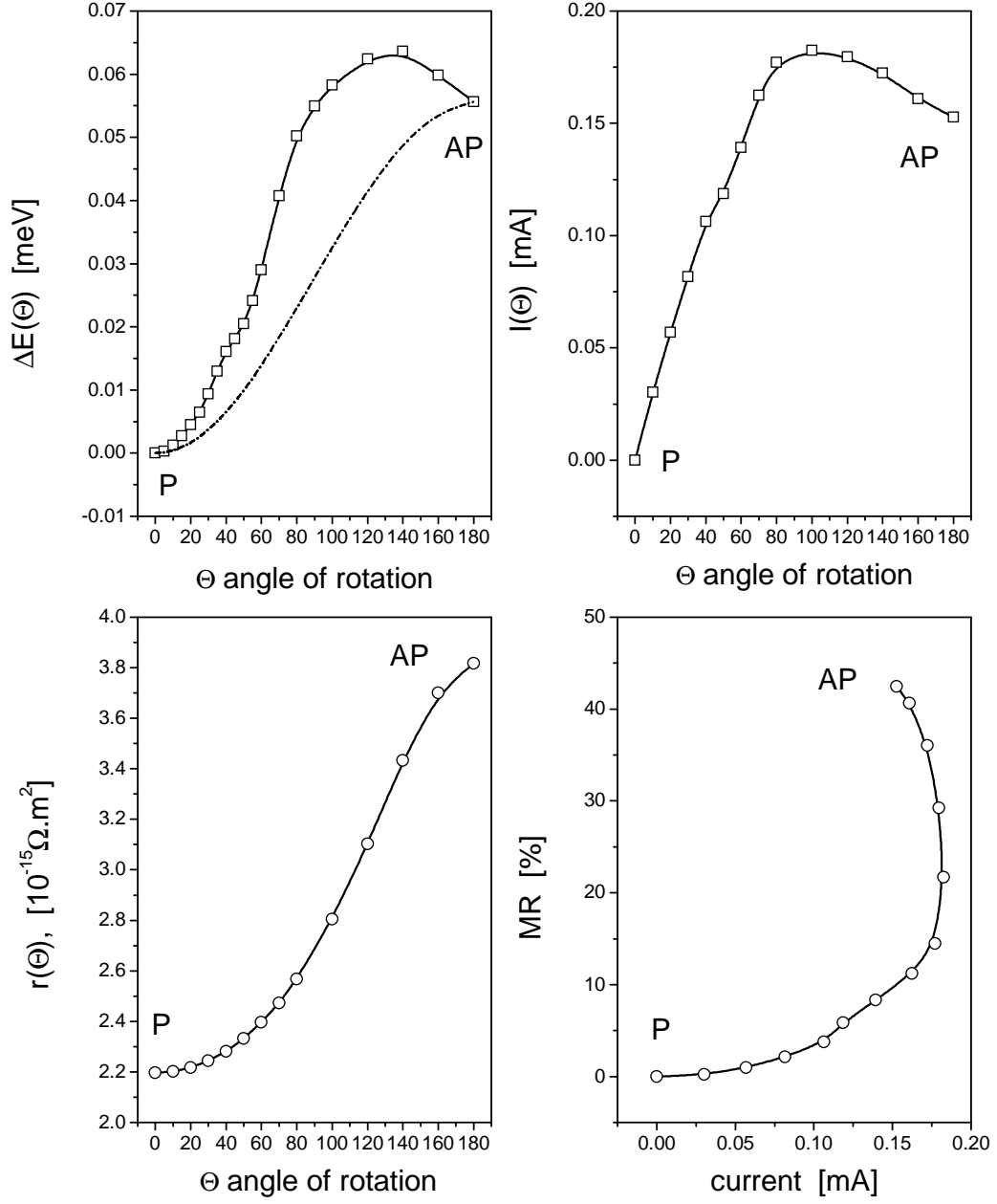


FIG. 4: Co/Cu₂₃/Co, spacer thickness: 39.85 Å. Left column: twisting energy and sheet resistance as a function of the rotation angle Θ . The dashed-dotted line refers to the first order approximation for the twisting energy. Right column: current as a function of the rotation angle Θ (top) and magnetoresistance as a function of the current (bottom), $\sqrt{\langle A_0 \rangle_{\text{SI}} / \langle \tau_{\text{min}} \rangle_{\text{SI}}} = 1$, see Eq.(44). Solid lines serve as guidance for the eye.

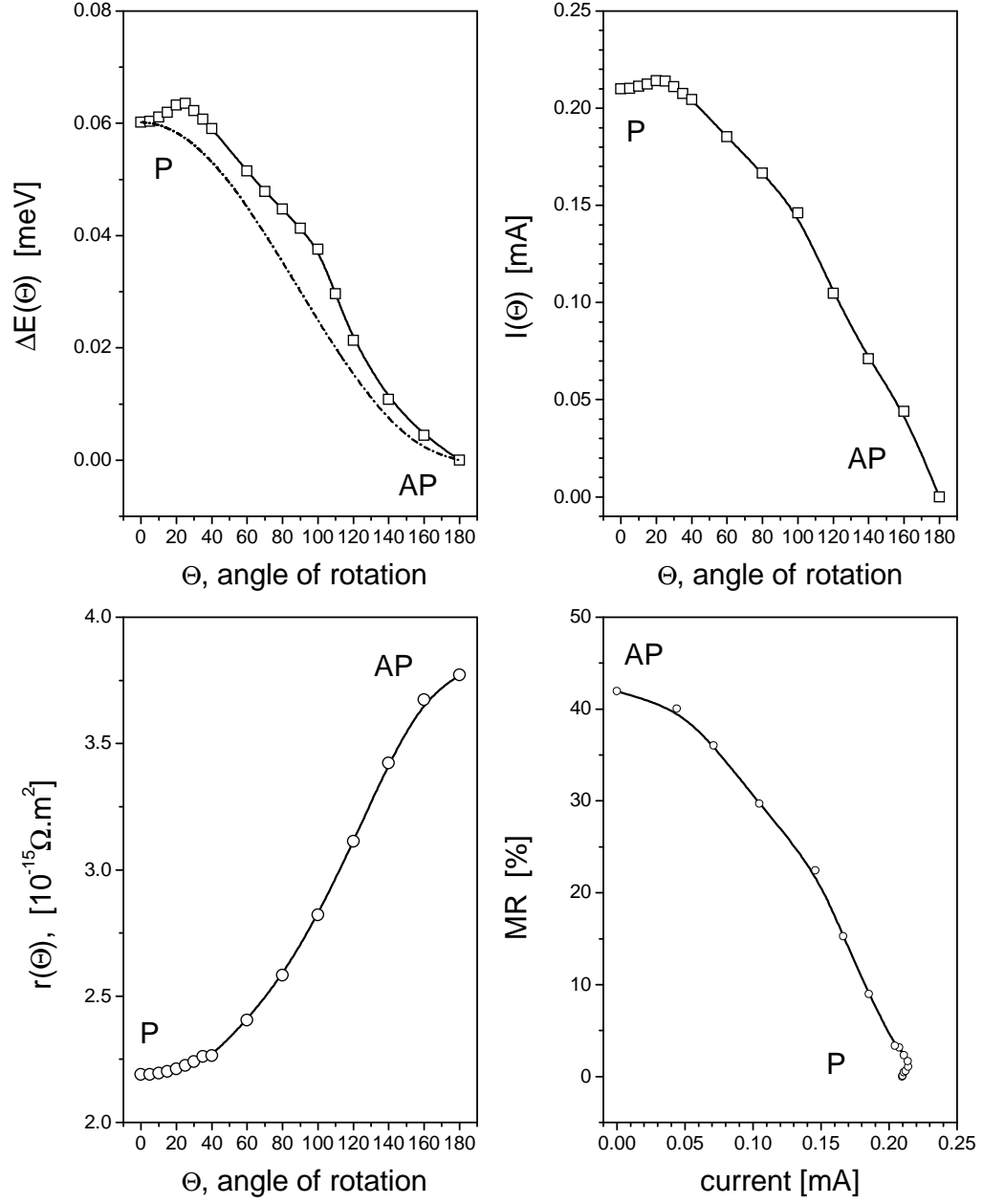


FIG. 5: Co/Cu₂₄/Co, spacer thickness: 41.58 Å. Left column: twisting energy and sheet resistance as a function of the rotation angle Θ . The dashed-dotted line refers to the first order approximation for the twisting energy. Right column: current as a function of the rotation angle Θ (top) and magnetoresistance as a function of the current (bottom), $\sqrt{\langle A_0 \rangle_{\text{SI}} / \langle \tau_{\text{min}} \rangle_{\text{SI}}} = 1$, see Eq.(44). Solid lines serve as guidance for the eye.

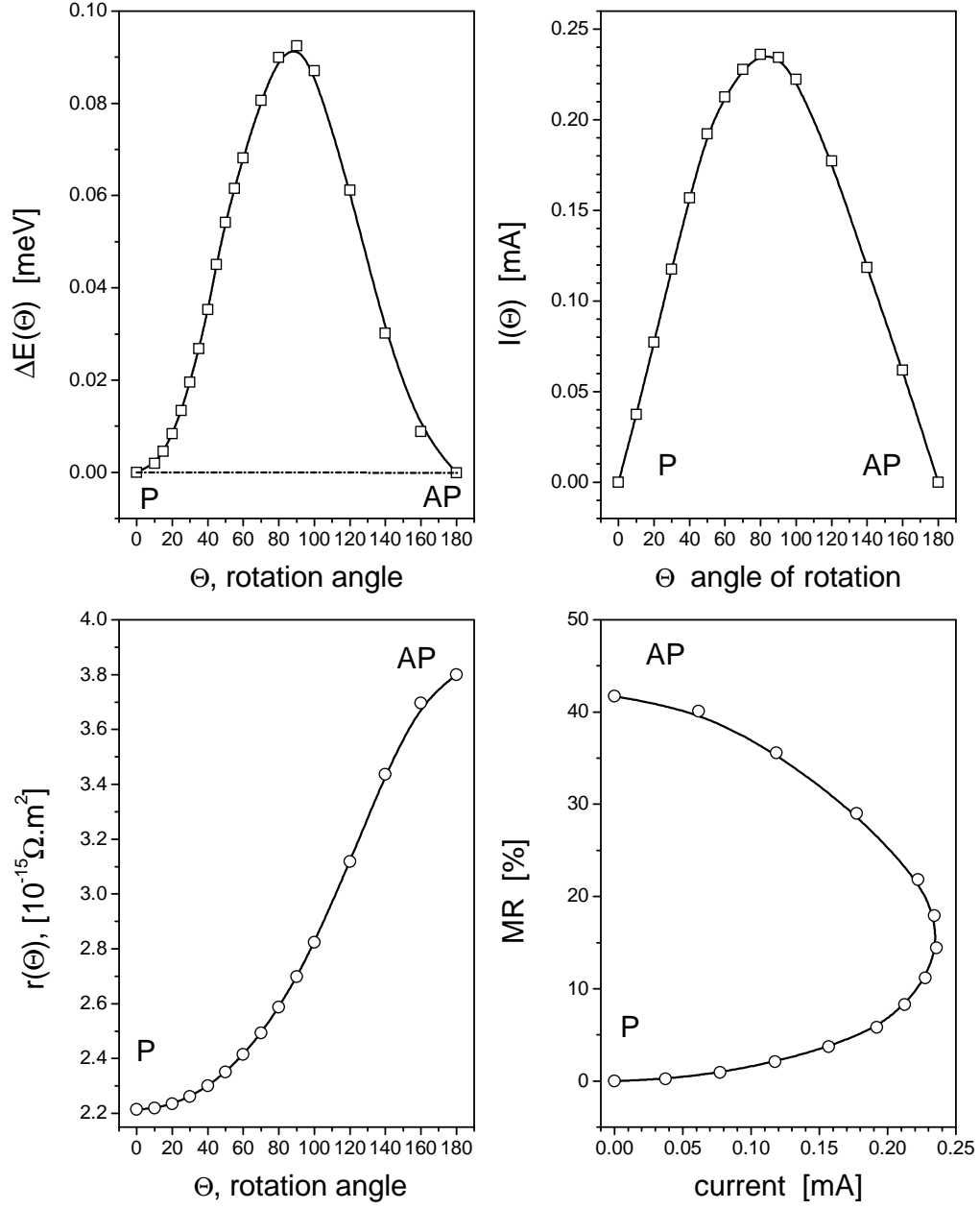


FIG. 6: Co/Cu₂₅/Co, spacer thickness: 43.32 Å. Left column: twisting energy and sheet resistance as a function of the rotation angle Θ . The dashed-dotted line refers to the first order approximation for the twisting energy. Right column: current as a function of the rotation angle Θ (top) and magnetoresistance as a function of the current (bottom), $\sqrt{\langle A_0 \rangle_{\text{SI}} / \langle \tau_{\text{min}} \rangle_{\text{SI}}} = 1$, see Eq.(44). Solid lines serve as guidance for the eye.

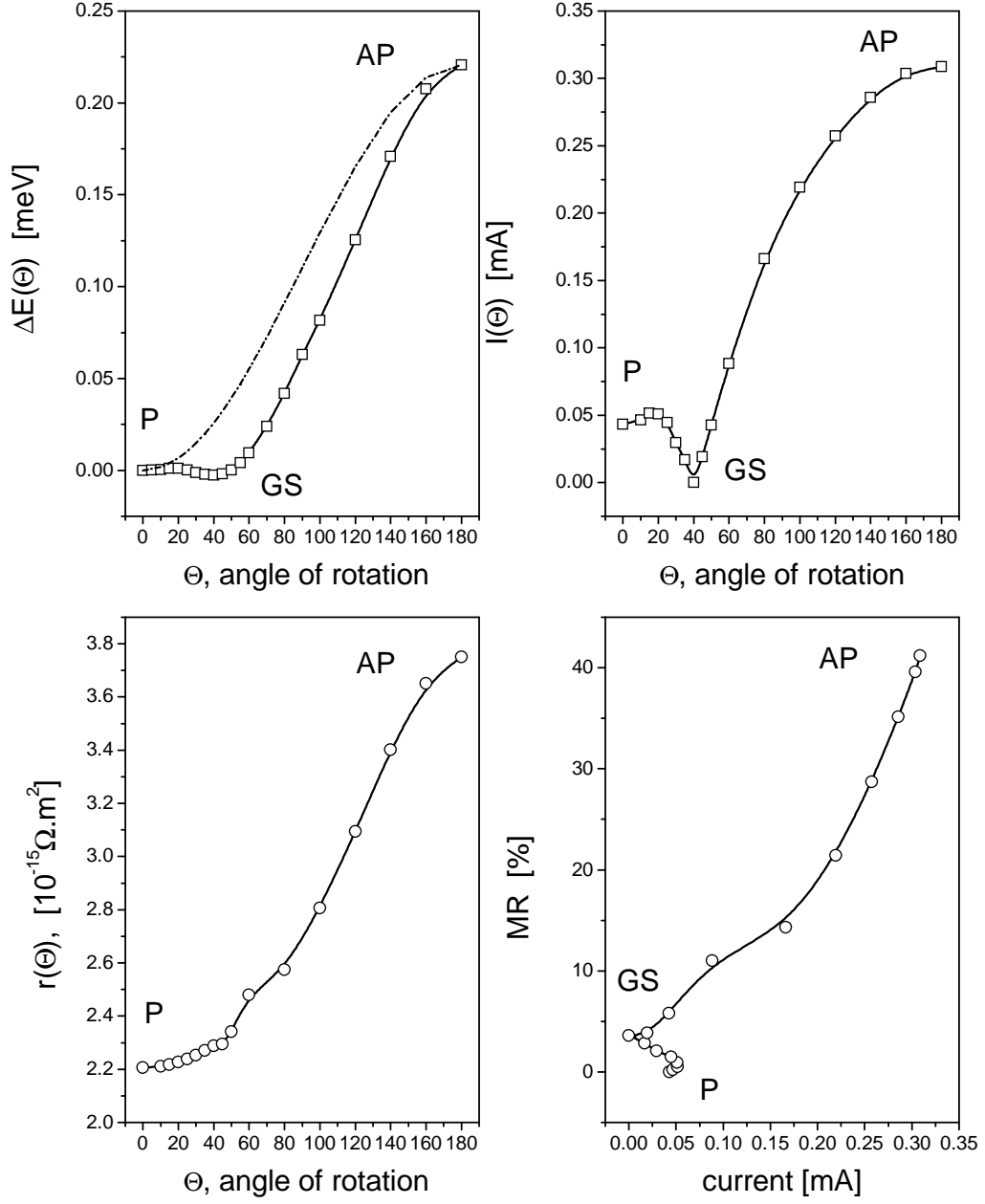


FIG. 7: Co/Cu₂₆/Co, spacer thickness: 45.05 Å. Left column: twisting energy and sheet resistance as a function of the rotation angle Θ . The dashed-dotted line refers to the first order approximation for the twisting energy. Right column: current as a function of the rotation angle Θ (top) and magnetoresistance as a function of the current (bottom), $\sqrt{\langle A_0 \rangle_{\text{SI}} / \langle \tau_{\text{min}} \rangle_{\text{SI}}} = 1$, see Eq.(44). Solid lines serve as guidance for the eye.

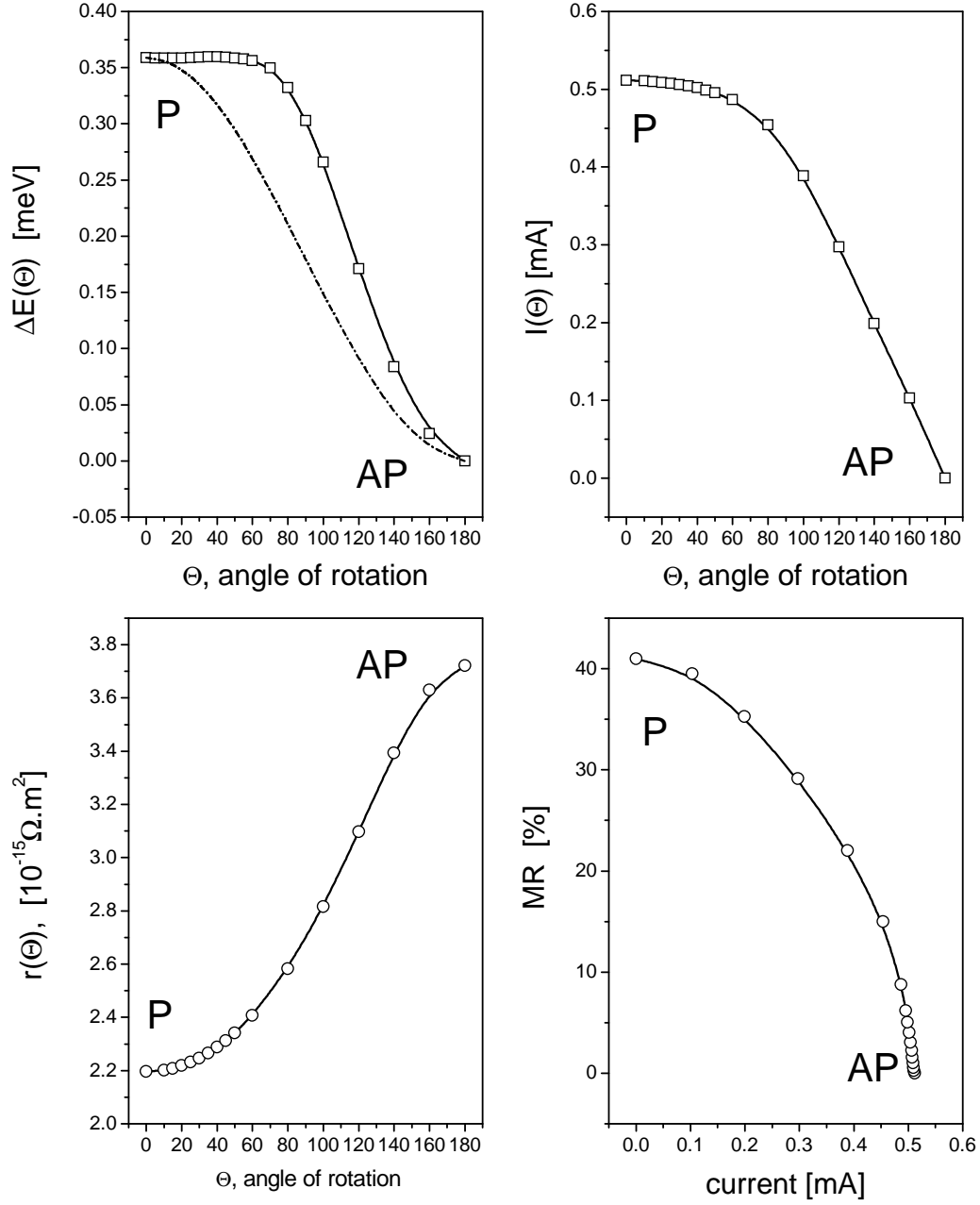


FIG. 8: Co/Cu₂₇/Co, spacer thickness: 46.78 Å. Left column: twisting energy and sheet resistance as a function of the rotation angle Θ . The dashed-dotted line refers to the first order approximation for the twisting energy. Right column: current as a function of the rotation angle Θ (top) and magnetoresistance as a function of the current (bottom), $\sqrt{\langle A_0 \rangle_{\text{SI}} / \langle \tau_{\text{min}} \rangle_{\text{SI}}} = 1$, see Eq.(44). Solid lines serve as guidance for the eye.

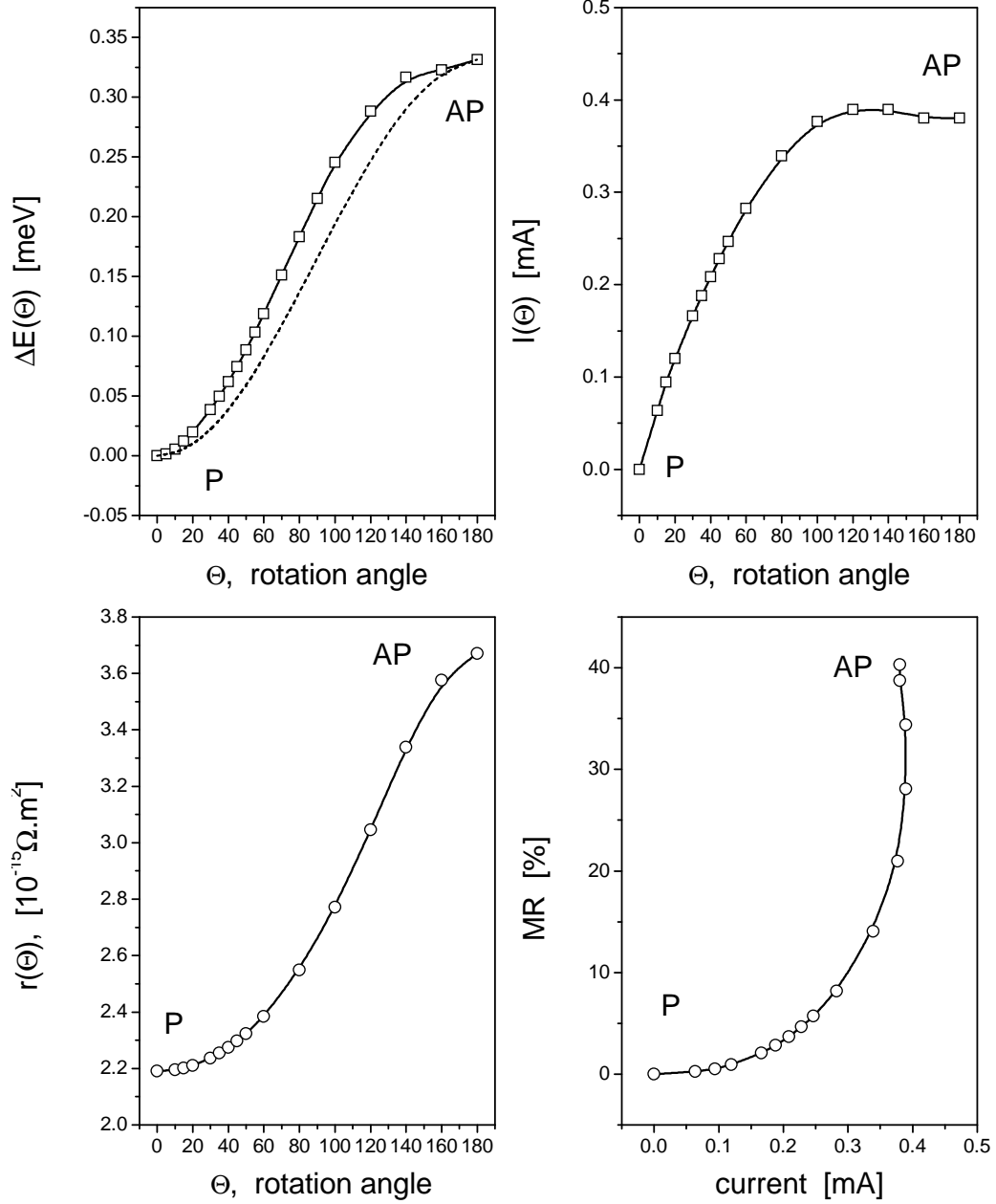


FIG. 9: Co/Cu₂₈/Co, spacer thickness: 48.51 Å. Left column: twisting energy and sheet resistance as a function of the rotation angle Θ . The dashed-dotted line refers to the first order approximation for the twisting energy. Right column: current as a function of the rotation angle Θ (top) and magnetoresistance as a function of the current (bottom), $\sqrt{\langle A_0 \rangle_{SI} / \langle \tau_{min} \rangle_{SI}} = 1$, see Eq.(44). Solid lines serve as guidance for the eye.

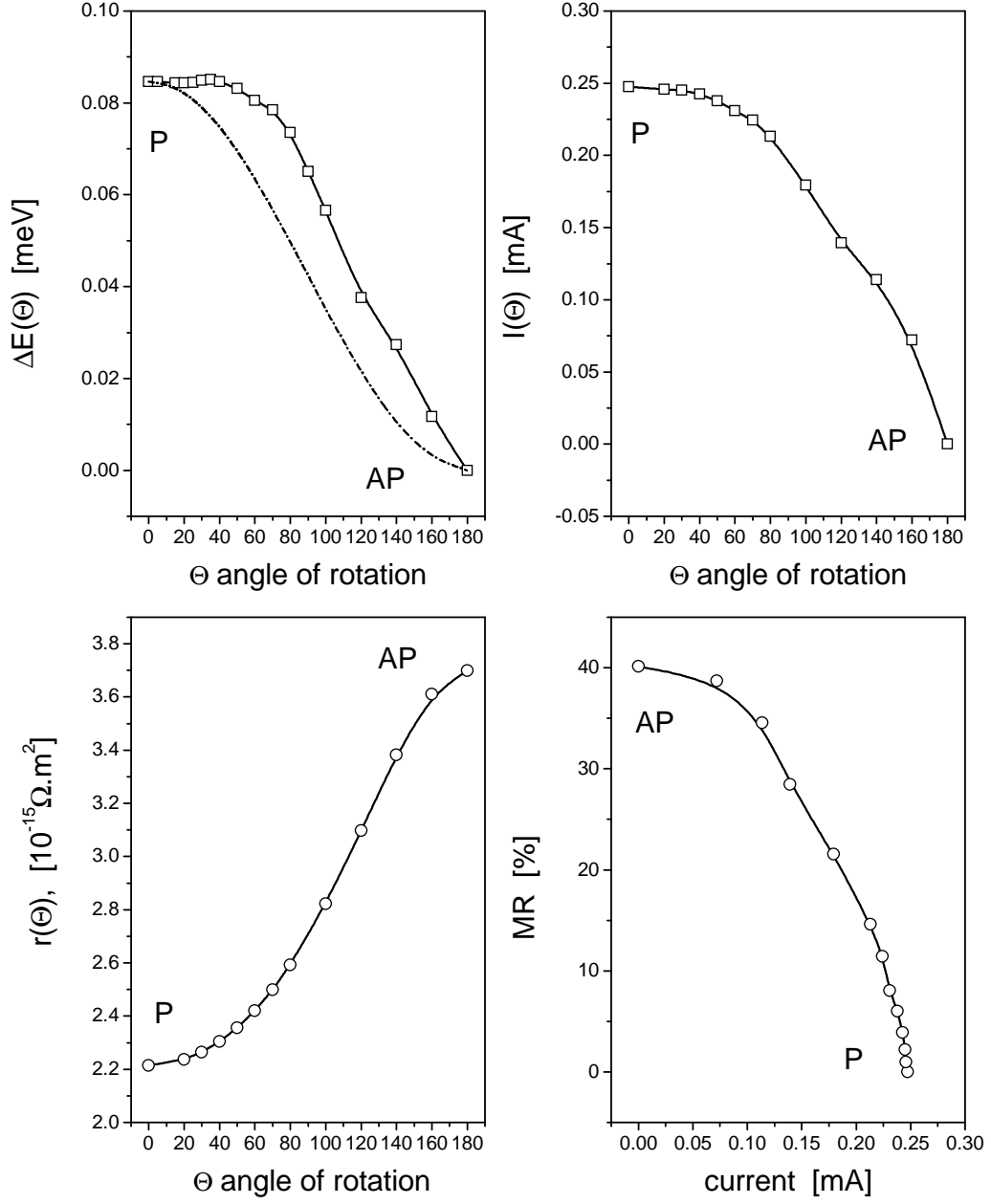


FIG. 10: Co/Cu₂₉/Co, spacer thickness: 50.24 Å. Left column: twisting energy and sheet resistance as a function of the rotation angle Θ . The dashed-dotted line refers to the first order approximation for the twisting energy. Right column: current as a function of the rotation angle Θ (top) and magnetoresistance as a function of the current (bottom), $\sqrt{\langle A_0 \rangle_{\text{SI}} / \langle \tau_{\text{min}} \rangle_{\text{SI}}} = 1$, see Eq.(44). Solid lines serve as guidance for the eye.

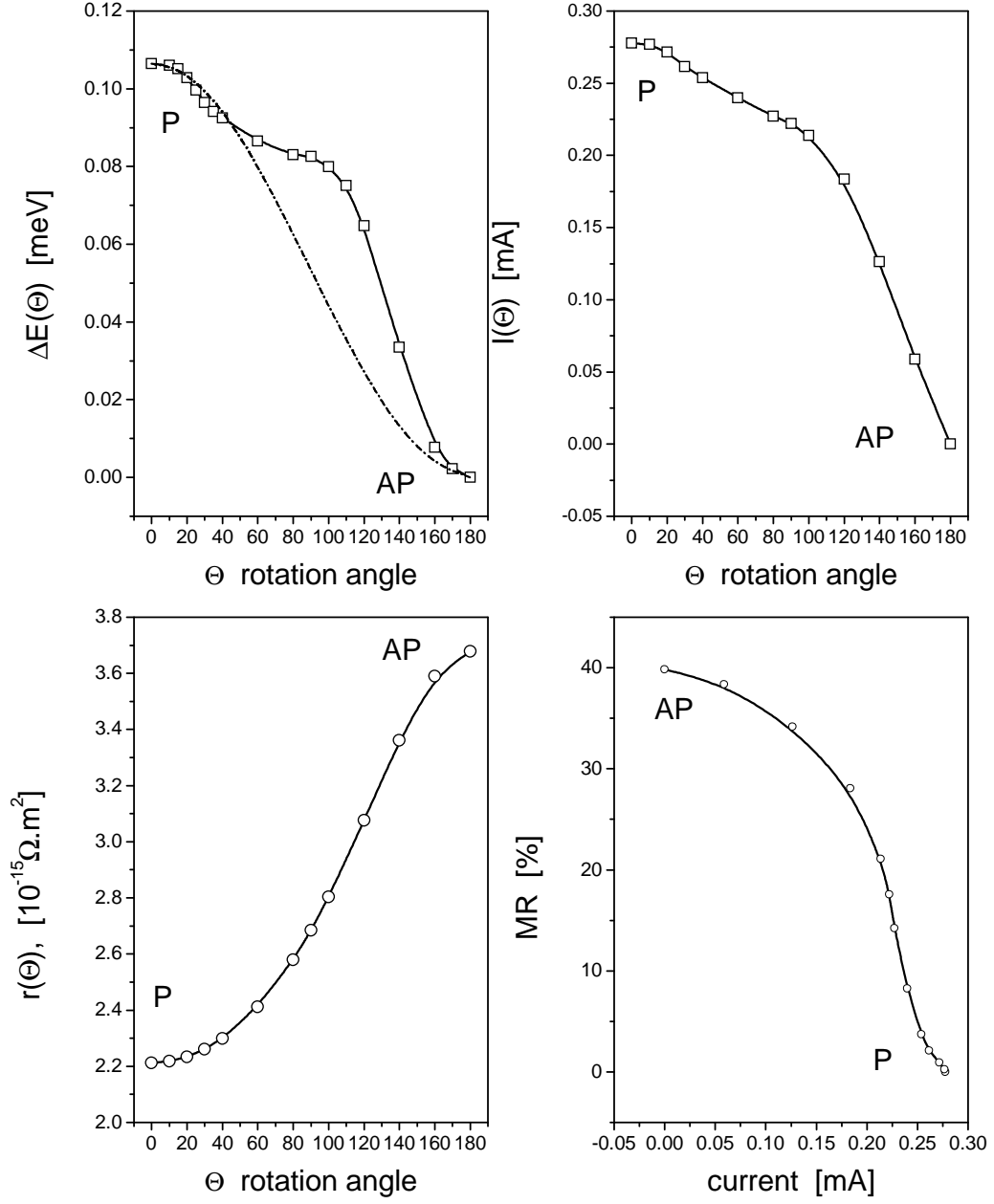


FIG. 11: Co/Cu₃₀/Co, spacer thickness: 51.98 Å. Left column: twisting energy and sheet resistance as a function of the rotation angle Θ . The dashed-dotted line refers to the first order approximation for the twisting energy. Right column: current as a function of the rotation angle Θ (top) and magnetoresistance as a function of the current (bottom), $\sqrt{\langle A_0 \rangle_{\text{SI}} / \langle \tau_{\text{min}} \rangle_{\text{SI}}} = 1$, see Eq.(44). Solid lines serve as guidance for the eye.

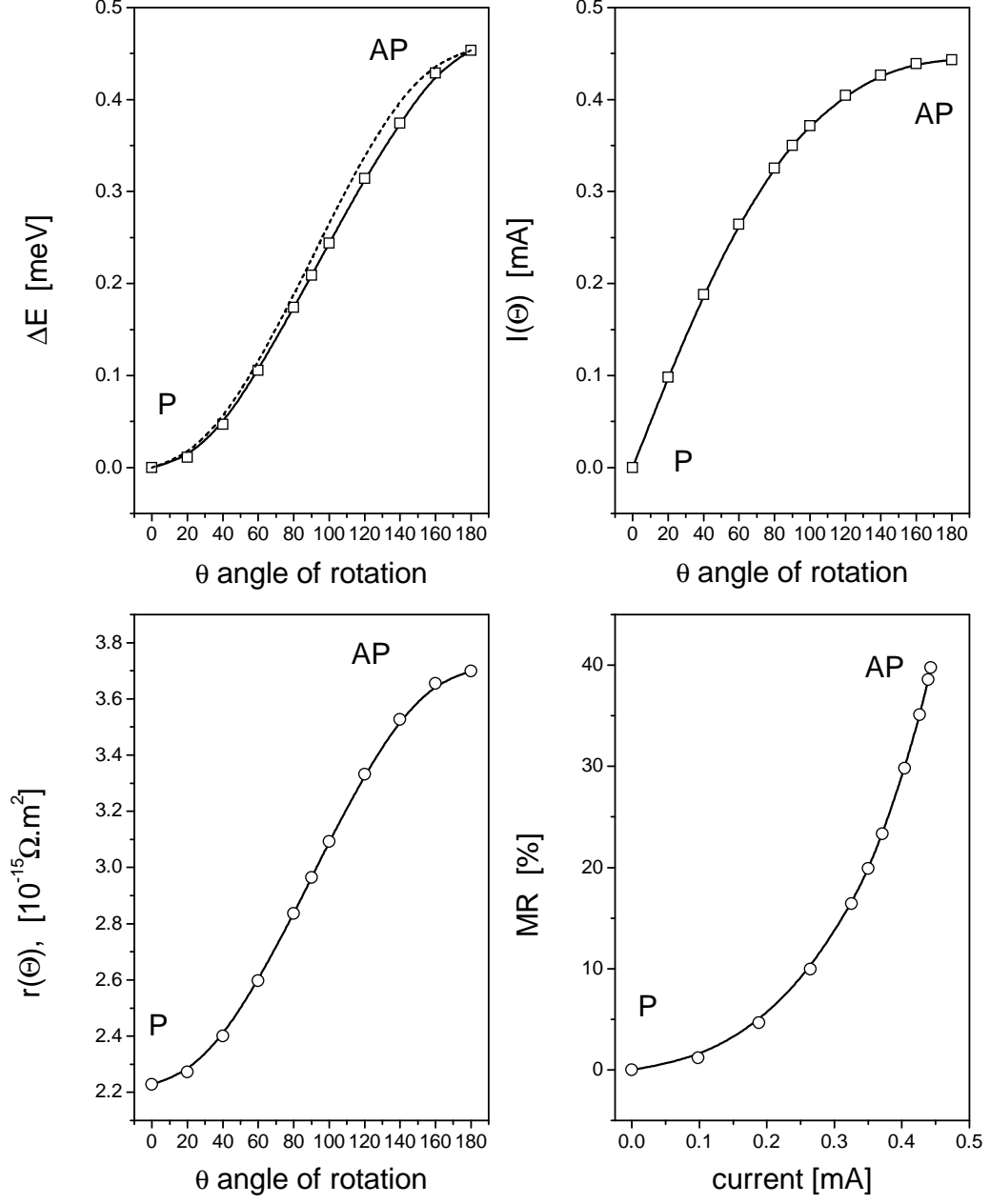


FIG. 12: Co/Cu₃₁/Co, spacer thickness: 53.71 Å. Left column: twisting energy and sheet resistance as a function of the rotation angle Θ . The dashed-dotted line refers to the first order approximation for the twisting energy. Right column: current as a function of the rotation angle Θ (top) and magnetoresistance as a function of the current (bottom), $\sqrt{\langle A_0 \rangle_{SI} / \langle \tau_{\min} \rangle_{SI}} = 1$, see Eq.(44). Solid lines serve as guidance for the eye.

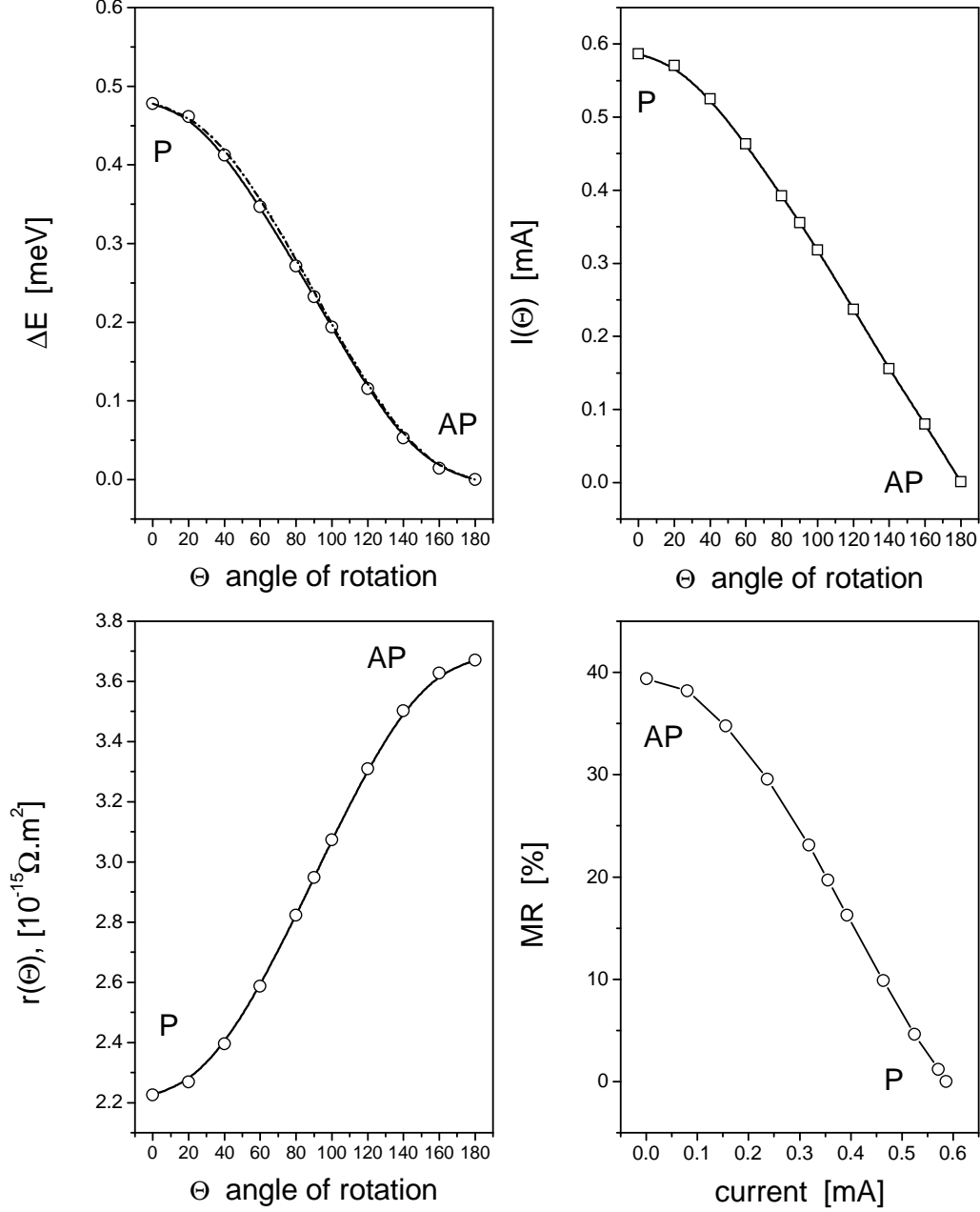


FIG. 13: Co/Cu₃₂/Co, spacer thickness: 55.45 Å. Left column: twisting energy and sheet resistance as a function of the rotation angle Θ . The dashed-dotted line refers to the first order approximation for the twisting energy. Right column: current as a function of the rotation angle Θ (top) and magnetoresistance as a function of the current (bottom), $\sqrt{\langle A_0 \rangle_{\text{SI}} / \langle \tau_{\text{min}} \rangle_{\text{SI}}} = 1$, see Eq.(44). Solid lines serve as guidance for the eye.

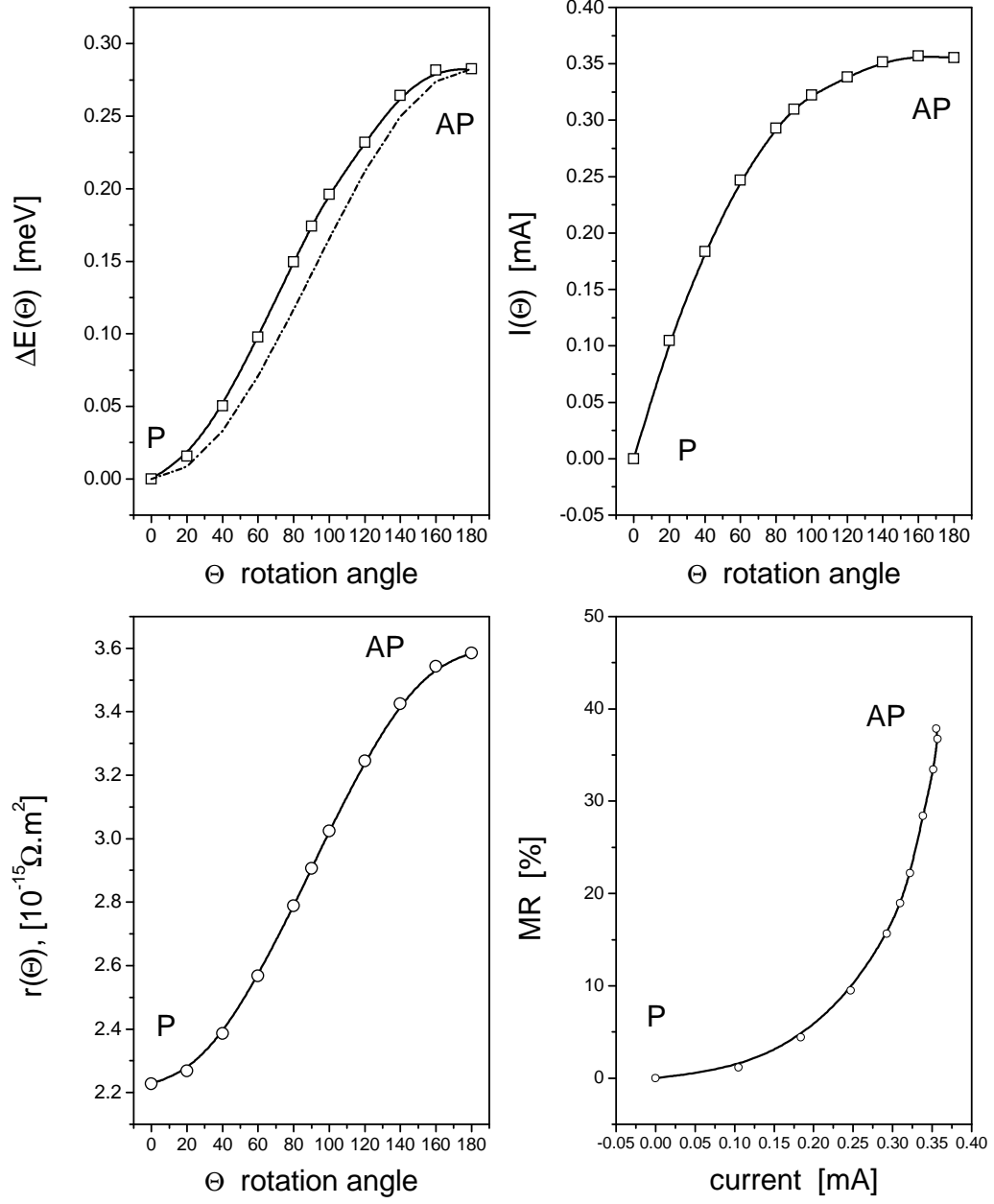


FIG. 14: Co/Cu₃₃/Co, spacer thickness: 57.18 Å. Left column: twisting energy and sheet resistance as a function of the rotation angle Θ . The dashed-dotted line refers to the first order approximation for the twisting energy. Right column: current as a function of the rotation angle Θ (top) and magnetoresistance as a function of the current (bottom), $\sqrt{\langle A_0 \rangle_{\text{SI}} / \langle \tau_{\text{min}} \rangle_{\text{SI}}} = 1$, see Eq.(44). Solid lines serve as guidance for the eye.

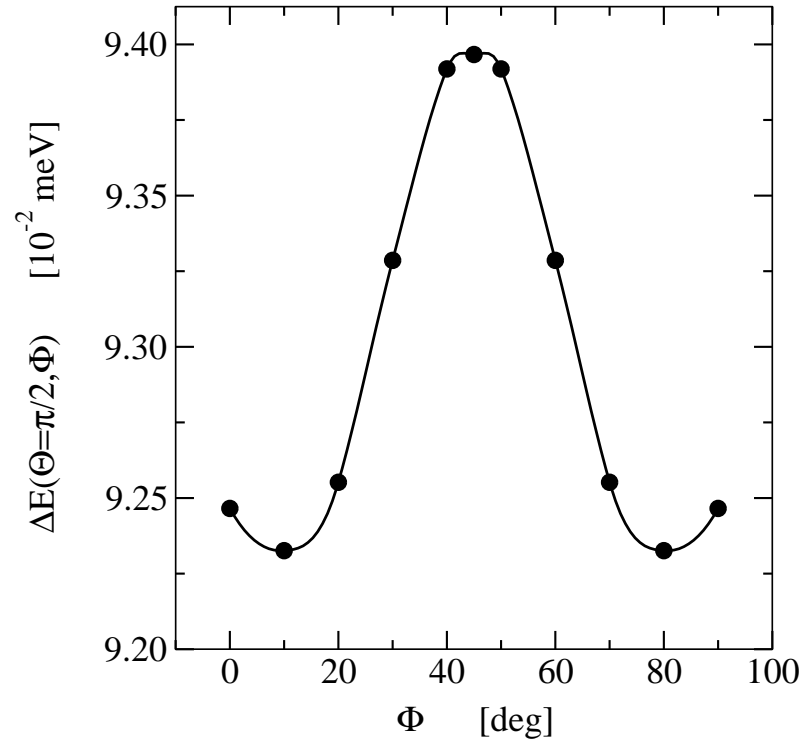
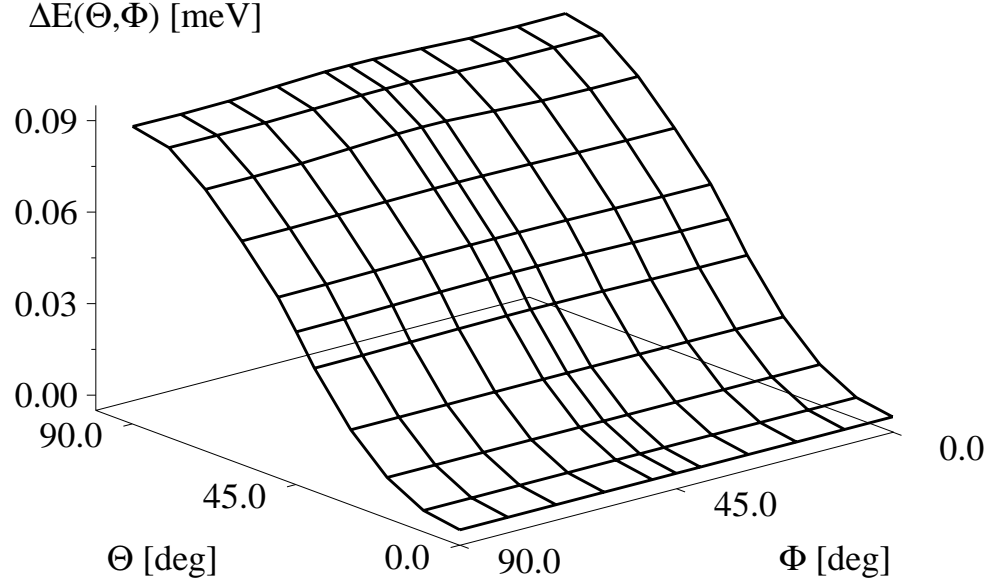


FIG. 15: Top: Twisting energy as a function of both rotation angles for the system with 25 spacer layers of Cu. Bottom: precessional energy at $\Theta = 90^\circ$.